coatings

MDPI

Article

Study on the Construction of Dynamic Modulus Master Curve of Polyurethane Mixture with Dense Gradation

Haisheng Zhao [1,2], Wenbin Gao [3], Shiping Cui [1], Wensheng Zhang [4], Shijie Ma [1,*], Baoji Miao [4], Chunhua Su [1], Jincheng Wei [1], Shan Liu [1] and Fuxiu Liu [1]

[1] Key Laboratory of Highway Maintain Technology Ministry of Communication, Jinan 250102, China; zhaohaisheng@sdjtky.cn (H.Z.)
[2] School of Highway, Chang'an University, Xi'an 710064, China
[3] Yantai Highway Development Center, Yantai 264000, China
[4] Wanhua Chemical Group Co., Ltd., Yantai 265599, China
* Correspondence: mashijie@sdjtky.cn; Tel.: +86-18660163082

Abstract: The PU mixture considered here is a new kind of pavement material with excellent road performance, which lacks study into its dynamic mechanical and viscoelastic properties. In this study, the dynamic modulus of the polyurethane (PU) mixture was fitted by using five master curve models, five shift factor equations, and four error minimization methods. According to test results, the log–log plot form was able to more effectively display the differences between master curves. The solver method, the sum of square error minimization ($\leq$0.02), proved to be more appropriate and accurate with higher fitting parameter results. The line of equality statistic and Pearson linear correlation analysis results demonstrated that WLF and Kaelble equations were appropriate for five master curve models with trend line R^2 values higher than 0.98. The GLS and SCM model with the WLF equation had the most accurate master curve fitting results. The dynamic modulus master curve shape of the PU mixture did not follow the traditional smooth "S" shape and did not show the ultimate dynamic modulus at extreme frequency. The viscoelasticity of the PU mixture is quite different from that of the asphalt mixture. This study recommended the most accurate error minimization method, the master curve model, and shift factor equations for characterizing the dynamic properties of the PU mixture.

Keywords: polyurethane mixture; dynamic modulus; master curve model; shift factor equation; error minimization

check for updates

Citation: Zhao, H.; Gao, W.; Cui, S.; Zhang, W.; Ma, S.; Miao, B.; Su, C.; Wei, J.; Liu, S.; Liu, F. Study on the Construction of Dynamic Modulus Master Curve of Polyurethane Mixture with Dense Gradation. *Coatings* **2023**, *13*, 835. https://doi.org/10.3390/coatings13050835

Academic Editor: Sharareh Shirzad

Received: 29 March 2023
Revised: 22 April 2023
Accepted: 25 April 2023
Published: 26 April 2023

Copyright: © 2023 by the authors. Licensee MDPI, Basel, Switzerland. This article is an open access article distributed under the terms and conditions of the Creative Commons Attribution (CC BY) license (https://creativecommons.org/licenses/by/4.0/).

1. Introduction

When an asphalt mixture is subjected to dynamic loading and the amplitude of the dynamic loading can maintain the strain within 100 με, the asphalt mixture will exhibit a complex linear viscoelastic behavior [1–5] due to the combination of a viscoelastic asphalt binder and an aggregate skeleton. Before analyzing the material response [6,7] and pavement design [8,9], it is very critical to evaluate the rheological property of the asphalt mixture. The asphalt mixture's dynamic modulus and corresponding phase angle measurements will reveal important details about how the behavior of the material changes over time and loading [10,11].

In some circumstances (for example, excessively high temperature or extremely low loading frequency), it is difficult to measure the dynamic modulus of the asphalt mixture due to the limitations of the experimental equipment. In consideration of the time–temperature superposition principle (TTSP), it is essential to construct the master curve to extrapolate the dynamic modulus to temperature and frequency ranges that are unavailable at the laboratory level [12,13]. The test results can be extended to a wider extensive time–temperature space from certain loading frequencies and temperature ranges [14]. According to the TTSP, the master curve of a material with "thermos–rheologically simple" behavior is smooth and continuous [12,15,16].

The master curve is widely used to describe the viscoelastic and dynamic characteristics of the asphalt mixture. The master curve can be utilized to depict the fundamental dynamic properties of viscoelastic materials, including the dynamic modulus and phase angle. The dynamic modulus and phase angle could constitute the basis for understanding pavement load response and help to understand the behavior of the material under different temperatures and loading frequencies [8–11].

The laboratory–measured dynamic modulus of asphalt mixture is always shown in the form of the master curve over a wide range of temperatures and loading frequencies. A continuous master curve model could be used to fit the experimental test data into mathematical models [17]. The logistic sigmoidal equation [18,19], Weibull's equations [20], the modified Christensen–Anderson–Marasteanu (CAM) model [21], the Havriliak–Negami (HN) [22], and 2 Springs, 2 Parabolic creep elements, and 1 Dashpot (2S2P1D) models [17,23] were reported to develop different models for describing the dynamic modulus in master curve form. The widely accepted mathematical formulation for calculating the master curve of the asphalt mixture is the standard logistic sigmoidal–shaped (SLS) model due to its simplicity. Several advanced types of research were carried out to modify the SLS function [24–27]. The generalized logistic sigmoidal (GLS) model can be applied to fit asymmetric data, but the SLS model is more accurate for symmetrical test data [28,29]. Dickerson and Witt [30] established the relationship between a complex modulus, the phase angle, and the loading frequency of an asphalt binder and built the master curve of the dynamic modulus and phase angle by using independent parameters. Based on the simplification of the Dickerson and Witt model, Christensen and Anderson [11] developed the Christensen–Anderson (CA) model. Based on the CA model, Marasteanu and Anderson [21] established the Christensen–Anderson–Marasteanu (CAM) model, which fits the test data within extremely low or extremely high frequencies [21,31]. The study [32] employed five distinct master curve models to predict the dynamic modulus and corresponding phase angle for three different kinds of asphalt mixture, and recommended a model that combined the CAM model and sigmoidal model. Reference [33] adopted three master curve models and five kinds of shift equation factors to compare the prediction accuracy for four kinds of asphalt mixtures, and the SLS model and the Williams–Landel–Ferry equation produced the best–fitting results. Study [29] adopted two master curve models and three kinds of shift factor equations to construct the master curve model of the dynamic modulus, and the GLS model was proved to predict more precisely.

Some research work [23,34–38] compared different shift factor equations and analyzed the precision of dynamic modulus master curve models. Study [39–41] used the Williams–Landel–Ferry (WLF) equation and the Arrhenius equation to construct the dynamic modulus master curve. Study [42] proved that the Arrhenius shift factor equation had a lesser degree of freedom than the Polynomial and WLF shift factor equations, which led to the prediction accuracy of the Arrhenius shift factor equation decreasing especially at low temperatures. Reference [32] compared five different shift factor equations for fitting and predicting the experimental dynamic modulus and phase angle, and recommended a proper shift factor equation for generating the master curve. Study [33] adopted three shift factor equations and provided recommendations for the selection of the proper master curve model. References [43–45] utilized the Polynomial shift factor equation to construct the master curve of the asphalt mixture. Study [46] compared three shift factor equations (i.e., Arrhenius, WLF, log–linear) in the SLS model to build the master curve.

Several fitting techniques, such as the Artificial Neural Network (ANN), regression modeling, and modified least–square fitting approach, were employed in conjunction with analogical and numerical solutions to produce better fitting results and improve the precision of the prediction [8,35,47–49].

The dynamic modulus is widely used as an important input parameter in pavement structure design software, such as the Mechanistic–Empirical Pavement Design Guide (MEPDG). The dynamic modulus master curve reflects the dynamic mechanical performance and viscoelastic property of the asphalt mixture and is widely used in the area of asphalt mixture

and as an effective way to evaluate the asphalt mixture. Many studies [50,51] improved or modified the asphalt with a warm mix additive or other additives to improve the viscoelastic property under higher temperatures. The PU mixture which possesses good road performance [52,53] is a new kind of pavement material, the dynamic mechanical performance and viscoelastic properties of which should be captured and used to understand the performance of pavement structure with PU mixture layers before applying the PU mixture in pavement structure design, material selection, and performance prediction. Therefore, the dynamic modulus master curve study is one of the most important fundamental studies of the PU mixture. There is research [54] about the dynamic modulus master curve of the dense PU mixture, although only the SLS model was analyzed in this literature, and the SLS model exhibited a high level of goodness–of–fit. For this reason, there is an urgent need to study the construction of the dynamic modulus master curve of the PU mixture to provide more accurate information about the dynamic mechanical performance and viscoelastic of the PU mixture.

This paper aimed to adopt five different master curve models and five shift factor equations for fitting the dynamic modulus master curve of the PU mixture. Four different error–minimizing processes which would be used for obtaining the regression parameters of master curve models and shift factor equations were used in this paper. The results obtained were graphically and statistically analyzed and compared. This paper attempted to compare the different formulations and their effectiveness in the prediction of the dynamic modulus of the PU mixture. Finally, a simple and effective master curve model, shift factor equation, and error–minimizing processes are recommended for adjusting the dynamic modulus master curve for the entire range of reduced frequencies of the PU mixture for the following study.

2. Materials and Methods

2.1. Material

The PU mixture used in this study had dense gradation with basalt aggregate, and the gradation of the PU mixture was shown in Figure 1. The X and Y axes were in a 0.45 power scale and arithmetic scale, respectively.

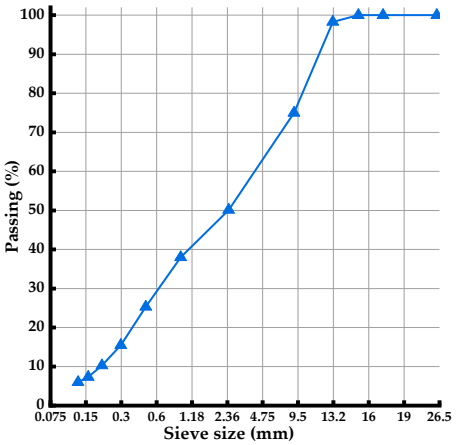


Figure 1. Gradation of PU mixture.

The optimum ratio of PU to aggregate was 5.3%, and the PU binder was supplied by Wanhua Chemical Group Co., Ltd. (Yantai, China). The PU binder would be solidified under wet conditions.

The specimen fabricating and dynamic modulus test both followed the procedure and requirements in the literature [55]. The fabricating of the specimens was as follows: the aggregate, filler, and PU binder were mixed at room temperature, and the PU mixture was kept at room temperature (below 30 °C) for 1.5 h before the compacting procedure. Then, the PU mixture was compacted 100 times by the Superpave gyratory compactor (SGC)

(Pine Test Equipment, Inc., Grove City, OH, USA), the dimensions of the specimen being about 170 mm in height and 150 mm in diameter. After compaction, the specimens were cured at 35 °C and 70% RH conditions for 5 days. After being cured, the specimens were cored and sawn into dimensions of 150 mm in height and 100 mm in diameter as required by AASHTO: TP–79 (2010).

The dynamic modulus test was performed on the Asphalt Mixture Performance Tester (AMPT), the control mode was strain control, and the loading waveform was sinusoidal. The strain of the specimens during the test procedure should be kept within 75–125 uε. The test temperatures were set at 5, 15, 25, 35, 45, and 55 °C, and the loading frequencies were set at 25, 20, 10, 5, 2, 1, 0.5, 0.2, and 0.1 Hz. The average dynamic modulus value of two replicates was used for the construction of the master curve.

2.2. Methodology

The dynamic modulus, which is measured at multiple temperatures and frequencies in the linear viscoelastic range, could be horizontally shifted to establish a single smooth and continuous master curve at the arbitrary reference temperature. The master curve which was constructed based on the theoretical base of TTSP was used to predict the viscoelastic behavior and to analyze the dynamic mechanical properties of the asphalt mixture at different loading frequencies and temperatures. 20 °C was adopted as the reference temperature in this study.

2.2.1. Dynamic Modulus Fitting Model

The dynamic modulus master curve of asphalt mixture could be described by certain mathematical models. In this paper, five models were adopted and shown as follows:

Model 1: Standard logistic sigmoidal model.

The Standard logistic Sigmoid model (SLS) [18] was introduced to (1) characterize the linear viscoelastic behaviors of the asphalt mixture with varying temperature and frequency; (2) fit the measured dynamic modulus, (3) construct the modulus master curve. The SLS model is given by Equation (1).

$$log(E^*) = \delta + \frac{\alpha}{1 + e^{\beta + \gamma \cdot log(f_r)}} \quad (1)$$

where E^* is the dynamic modulus in MPa; f_r is the load frequency at the reference temperature in Hz; δ, α, β, and γ are the fitting parameters. δ and $\delta + \alpha$ represent the minimum and maximum value of E^*; β and γ are the shape parameters of the model curve, which describes the shape of the SLS model as depicted in Figure 2. Equation (1) is a standard log function that provides a symmetrical shape to the evolution of dynamic modulus [9,29,48,56].

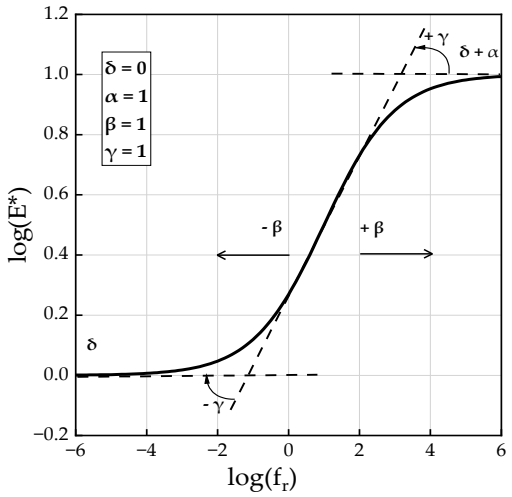


Figure 2. Graphical interpretation of the SLS model.

Model 2: Generalized logistic sigmoidal (GLS) model.

The SLS model presents a symmetrical shape and provides an excellent fit to symmetric measured data, but it is unable to fit non–symmetric curves acceptably. Due to the random heterogeneous characteristic of the asphalt mixture [25,57], the dynamic modulus results tend to exhibit an asymmetric pattern in most cases. Therefore, the GLS model was introduced by [58] to better characterize and fit the asymmetric development of dynamic modulus data. It is the general form of sigmoidal function applicable to fit asymmetric curves as can be seen in Equation (2).

$$lg(E^*) = \delta' + \frac{\alpha'}{\left[1 + \lambda \cdot e^{\beta' + \gamma \cdot lg(f_r)}\right]^{\frac{1}{\lambda}}} \quad (2)$$

where δ', α', β', and γ' are the fitting parameters; λ is the additional fitting parameter to take into account the asymmetric shape of the function; δ' and $\delta' + \alpha'$ represent the minimum and maximum value of E^*; β and γ describe the shape of the GLS model as depicted in Figure 3.

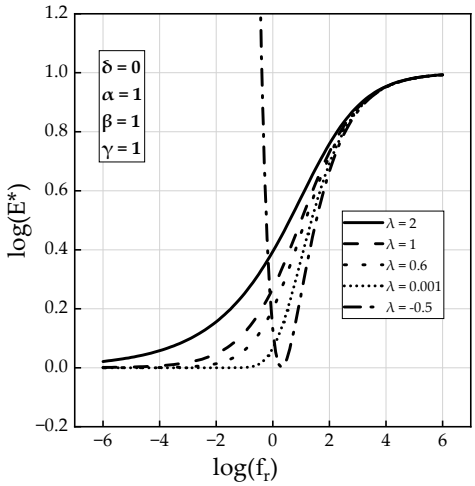


Figure 3. Graphical interpretation of GLS model.

Model 3: Christensen Anderson and Marasteanu model (1999) (CAM).

The Christensen–Anderson–Marasteanu (CAM) model was originally developed by Christensen (1998) [1] to describe the thermal rheological properties of the asphalt binder. Equation (3) presents the original CAM model for dynamic modulus.

$$log(E^*) = log(E_g) - \frac{w}{v} \cdot log\left[1 + (10^{log(f_r) - log(t_c)})^v\right] \quad (3)$$

where E_g is the Glassy modulus of asphalt mixture ranging from 45 to 50 GPa; f_r is the load frequency at the reference temperature in Hz; while v, w, and t_c are the fitting parameters.

It also should be mentioned that the CAM model (1999) [21,59] does not contain the sigmoidal structure in its mathematical expression. Equations (1) and (3) present an exponential–based function that provides a smooth "S"–shaped curve for data fitting. On the other hand, the CAM model presents [21] a combination of logarithm and exponential functions as can be seen in Equation (3) resulting in a deviation from an "S"–shaped pattern. Therefore, the shape of both dynamic modulus master curves may be remarkably different compared to those generated using Models 1 and 2.

Model 4: Modified CAM model.

Zeng and their co–authors introduced a modified version of the CAM model (Equation (4)) to better fit the dynamic modulus experimental data [60]. The modified CAM model consists of a power–law function within which additional fitting parameters were

introduced to generate master curves both for the asphalt binder and mixture. The master curve could be drawn by model fitting according to Equation (4).

$$E^*(f_r) = \delta + \frac{\alpha}{(1 + (f_c/f_r)^v)^{\frac{w}{v}}} \quad (4)$$

where δ and $\delta + \alpha$ are the equilibrium and glassy dynamic moduli, which represent the minimum and maximum modulus, respectively, estimated as regression; f_c is the location parameter with a dimension of frequency in Hz; while v and w are fitting parameters and describe the shape of the model as shown in Figure 4.

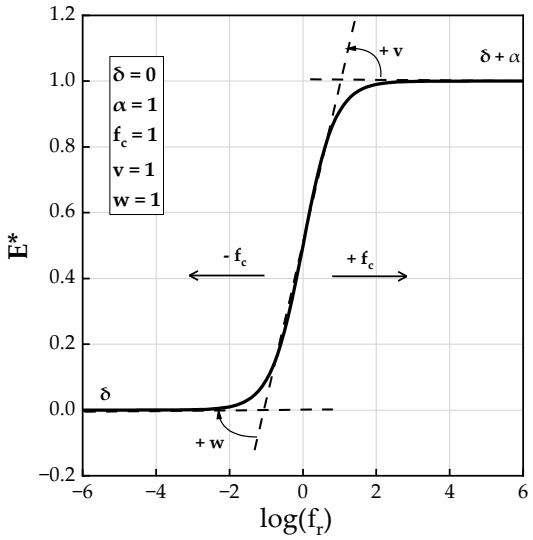


Figure 4. Graphical interpretation of modified CAM model.

It also should be mentioned that the CAM model (1999) [21,59] does not contain the sigmoidal structure in its mathematical expression. Equations (1) and (2) present an exponential–based function that provides a smooth "S"–shaped curve for data fitting. On the other hand, the CAM model [21] presents a combination of logarithm and exponential functions as can be seen in Equation (3) resulting in a deviation from an "S"–shaped pattern. Therefore, the shape of dynamic modulus master curves may be remarkably different compared to those generated using Models 1 and 2.

Model 5: Sigmoidal CAM Model (SCM model).

Given the mathematical limitations of the CAM models, a further modified version of the latter [21] is introduced in this paper by combining the simplicity and reasonable physical meaning (i.e., w means the velocity of phase angle and v represents the relaxation spectrum) of the CAM model with the benefit of the sigmoidal function. The model is named the Sigmoidal CAM Model (SCM) and can be described according to Equation (5).

$$log(E^*) = log(E_g) + \frac{w}{v} \cdot \frac{1}{\left(1 + e^{z \cdot log(f_r) + t_c}\right)^{\frac{1}{v}}} \quad (5)$$

where E_g, v, w, z, and t_c are consistent with the parameters of Model 3 (CAM model).

The SCM shows a similar basic mathematical structure to the modified sigmoidal function (see Equation (3)) while incorporating the conventional parameters of the original CAM model: glassy modulus; E_g, in GPa; parameter v, related to shape, slope, and limit value of the dynamic modulus; and parameters z, w, and t_c.

2.2.2. Shift Factor Equation

The dynamic modulus master curve construction requires that the data obtained at different temperatures and frequencies be related to each other to form a unique curve

of material stiffness. The shift factor is a function of temperature, which reflects the translation of the modulus curve at each temperature to form the master curve. The shift factor describes the temperature dependency of the dynamic modulus and the general form is given in Equation (6). It can be used to shift the dynamic modulus at different test temperatures to the reduced frequency of the master curve by applying the TTSP to constructing the master curve model. The reduced frequency f_r is the equivalent frequency of the experimental temperature concerning the reference temperature. Moreover, the reduced frequency can be obtained by Equation (6) once the shift factor is obtained.

$$f_r = f \cdot \alpha_T \tag{6}$$

$$log(f_r) = log(f) + log(\alpha_T) \tag{7}$$

where: log(f) is the frequency in experiment temperature; log(f_r) is the reduced frequency in reference temperature.

Five commonly used shift factor equations were adopted in this research: the log–linear equation, polynomial equation, Arrhenius equation, WLF equation, and Kaelble equation.

Equation (1): Log–linear equation.

The log–linear equation is one of the most popular temperature–shifting methods for asphalt mixtures. Christensen and Anderson [11] suggested that below 0 °C, log(α_T) varies linearly with temperature for many binders, and this same relationship has been deemed suitable for asphalt mixture at low to intermediate temperatures [61]. The log–linear equation for calculating the shift factor is:

$$log(\alpha_T) = C \cdot (T - T_r) \tag{8}$$

where α_T is the shift factor, T is the temperature, T_r is the reference temperature, and C is the constant which is determined by analysis of the measured data.

Equation (2): Polynomial equation.

The polynomial equation can fit the shift factors well over a wide range of temperatures and is expressed as:

$$log(\alpha_T) = a \cdot (T - T_r) + b \cdot (T - T_r)^2 \tag{9}$$

where a and b are regression parameters.

Equation (3): Arrhenius equation.

The Arrhenius equation for calculating the shift factor is presented in Equation (10):

$$log(\alpha_T) = \frac{E_a}{19.147142} \cdot \left(\frac{1}{T + 273.15} - \frac{1}{T_r + 273.15}\right) \tag{10}$$

where C is a constant. The Arrhenius equation has only one constant to be determined and can describe the behavior of the material below T_g [62].

Equation (4): Williams–Landel–Ferry equation.

The Williams–Landel–Ferry (WLF) equation is widely used to describe the relationship between shift factor and temperature above T_g and thereby assess the shift factor of asphalt mixtures:

$$log(\alpha_T) = \frac{-C_1 \cdot (T - T_r)}{C_2 + (T - T_r)} \tag{11}$$

where C_1 and C_2 are two regression parameters.

Equation (5): Kaelble equation.

The Kaelble equation is a modification of the WLF equation and can describe the relationship between shift factor and temperature below T_g as given in Equation (12).

$$log(\alpha_T) = \frac{-C_1 \cdot (T - T_r)}{C_2 + |T - T_r|} \tag{12}$$

where C_1 and C_2 are two regression parameters.

2.3. Goodness–of–Fit Statistics

The fundamental purpose of the regression–based model development process is to minimize the sum of the error from the prediction by comparing the predicted results with the measured results. The optimization process involves the determination of regression parameters in such a way that the development equation provides the minimum sum of the error, which is the difference between the predicted and measured results.

To construct the master curves deriving from the measured data, the nonlinear least–squares regression analysis was integrated into Microsoft Excel (Microsoft office 2019) Solver for the error–minimization process. The adjustment of the constants is carried out in such a way that the dynamic modulus master curve overlaps as closely as possible with the measured results.

To evaluate the divergence of fit between the five dynamic modulus models and minimize the error between predicted and measured dynamic modulus, "goodness–of–fit" is used in this study. Four different solver methods were applied to determine the "goodness–of–fit" [33]: the first (1) used Se/Sy (the ratio of the standard error (Se) to the standard deviation (Sy)) minimization, the second (2) used R^2 maximization, the third (3) used the Sum of Square Error (SSE) minimization, and the fourth (4) used $Error^2$ minimization.

The standard error of estimation and standard error of deviation is defined as follows [63]:

$$Se = \sqrt{\frac{1}{(n-p-1)} \cdot \sum_{i}^{n} |\hat{x}_i - x_i|^2} \tag{13}$$

$$Sy = \sqrt{\frac{1}{(n-1)} \cdot \sum_{i}^{n} |\hat{x}_i - \overline{x}_i|^2} \tag{14}$$

where x_i is the measured dynamic modulus in MPa, $\hat{x}_i$ is the predicted dynamic modulus in MPa, and $\overline{x}_i$ is the mean value of the measured dynamic modulus in MPa.

The standard error ratio and coefficient of determination (R^2) were used to evaluate the goodness–of–fit between measured and predicted values. To compute the error, the R^2 of a given model can be obtained using Equation (15):

$$R^2 = 1 - \frac{(n-p-1) \cdot S_e^2}{(n-1) \cdot S_y^2} \tag{15}$$

where n is the sample size, and p is the number of parameters to be estimated.

The Sum of Square Error (SSE) between measured values after shifting as shown in Equation (16) was used for the fitting procedure.

$$SSE = \sum \frac{(|E^*|_{measured} - |E^*|_{predicted})^2}{(|E^*|_{measured})^2} \tag{16}$$

where $|E^*|_{measured}$ is the experimental measured dynamic modulus in MPa, and $|E^*|_{predicted}$ is the predicted dynamic modulus predicted by different master curve models and shift factor equations in MPa. The SSE parameter could represent the relative error between the predicted and experimental measured dynamic modulus.

To define the optimal results of master curves, the coefficients of the models and shift factor equations were fitted to minimize SSE.

A simultaneous minimization approach can be performed to fit the experimental results as can be seen in Equation (17).

$$Error^2 = \sum_{i=1}^{n} \left[|E^*|_{measured} - |E^*|_{predicted} \right]^2 \tag{17}$$

where the parameters of this equation are the same as mentioned above. The Error^2 parameter reflects the absolute error between the predicted and experimental–measured dynamic modulus.

3. Results

3.1. Analyzing Master Curve Scale Type

The relationship between the dynamic modulus and loading frequency could be plotted in many scale types, e.g., logarithmic scale [64,65], arithmetic scale [66], and semi–logarithmic.

On the logarithmic scale, the loading frequency on the *x*–axis and the dynamic modulus on the *y*–axis is in log form. On the arithmetic scale, the loading frequency on the *x*–axis and the dynamic modulus on the *y*–axis are in natural numbers. On the semi–logarithmic, one of the axes is in log form, the other axis is in natural numbers.

The SLS model was adopted as an example to compare the difference between different scale types. The master curves fitted by the SLS model results which were plotted in different scale types are shown in Figure 5.

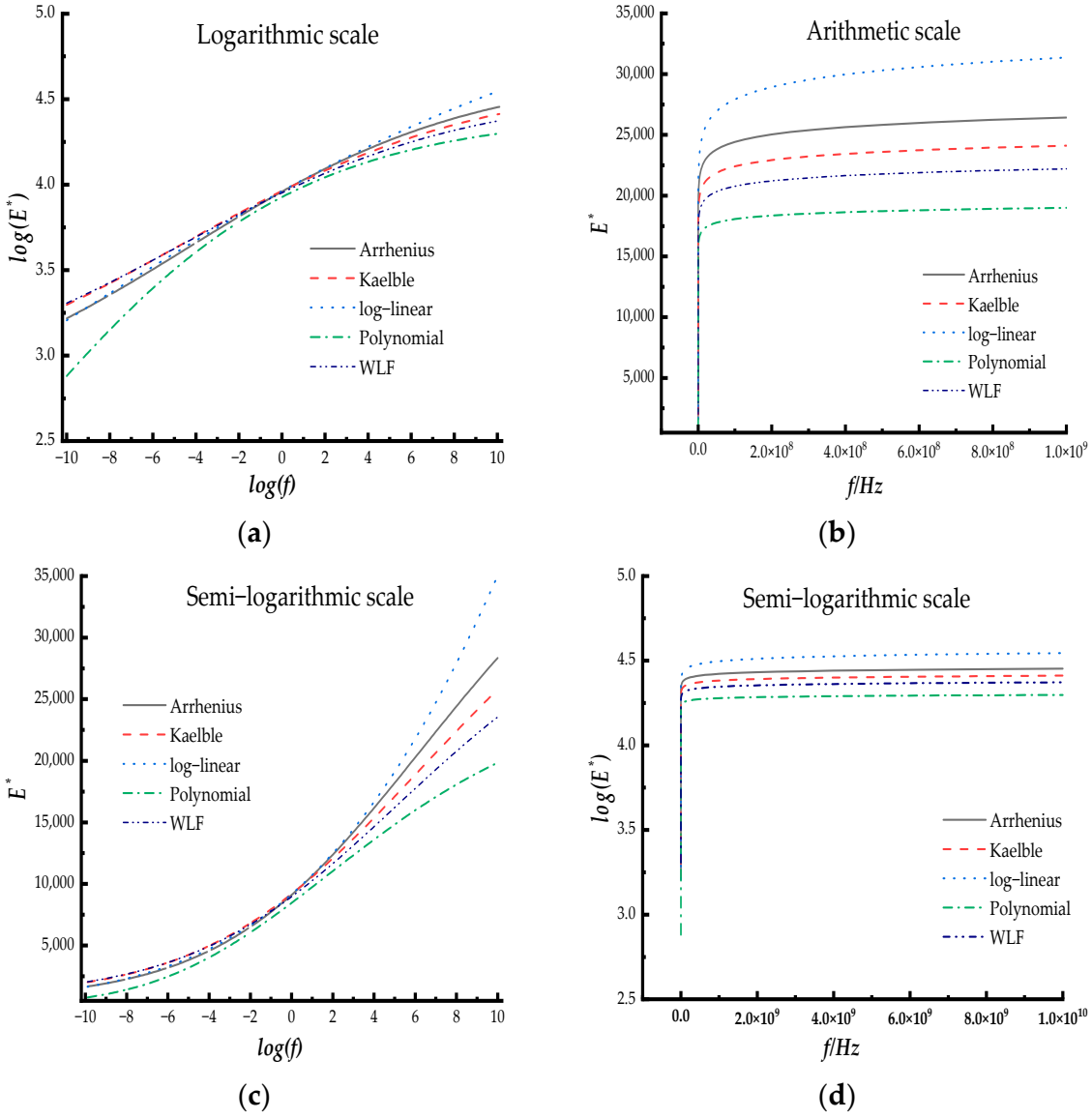


Figure 5. SLS model results at different scale types. (**a**) logarithmic scale; (**b**) arithmetic scale; (**c**) *x* axis in logarithmic scale; (**d**) *y* axis in logarithmic scale.

3.2. Analyzing the Influence of the Solver Method on the Fitting of the Dynamic Modulus Master Curve

3.2.1. The SLS Model Fitting Results Analysis

The dynamic modulus master curve fitting results of the SLS model along with five different shift factor equations and four solver methods are plotted in Figure 6. For further comparison, the fitting results of five different shift factor equations under the same solver method are shown in a single plot.

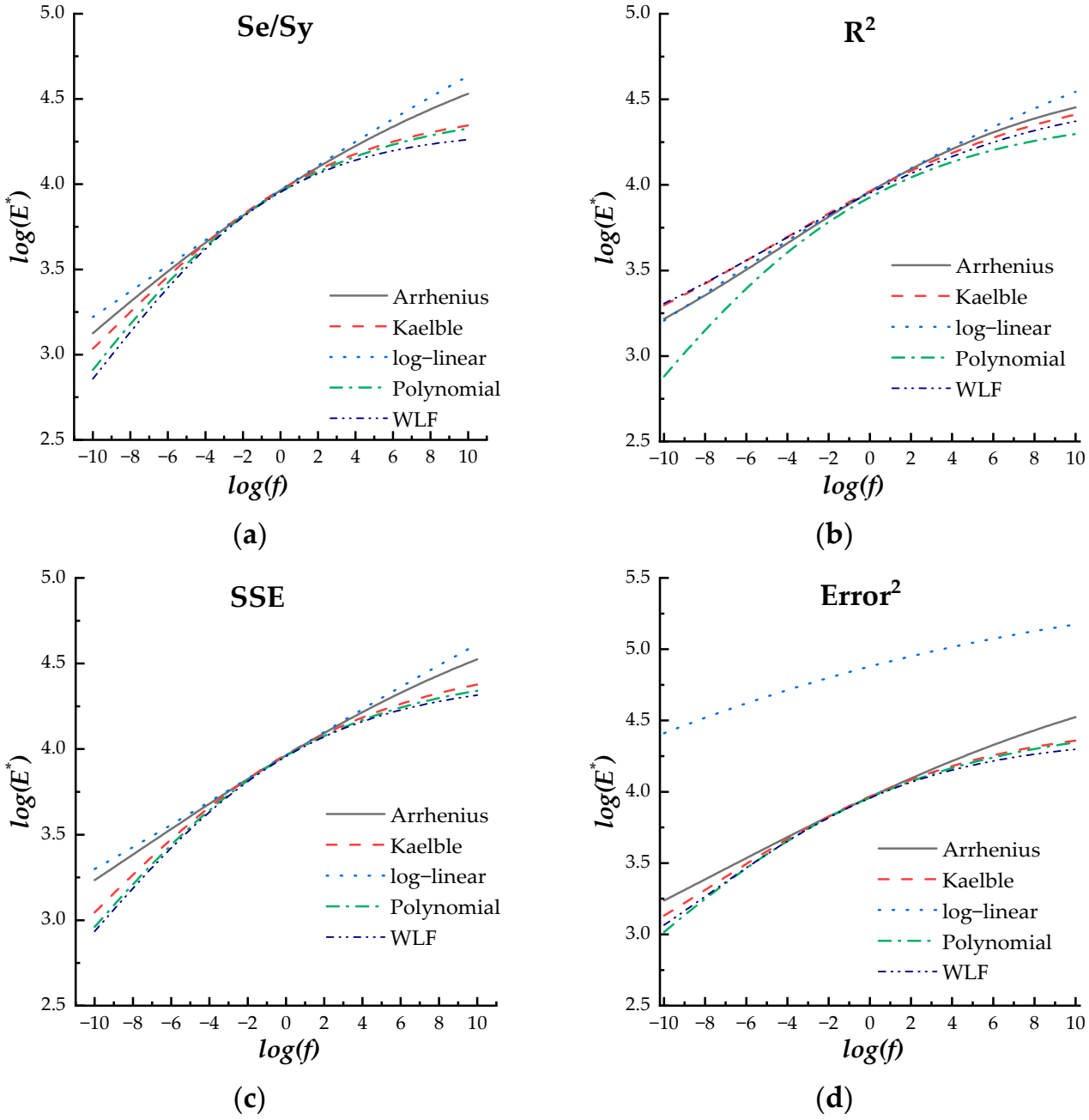


Figure 6. The master curve of SLS model fitting results with different shift factor equations. (**a**) Se/Sy minimization; (**b**) R^2 maximization; (**c**) SSE minimization; (**d**) $Error^2$ minimization.

3.2.2. The GLS Model Fitting Results Analyzing

Figure 7 shows the results of dynamic modulus master curve fitting using the GLS model along with five different shift factor equations and four solver methods. For further

comparison, the fitting results of five different shift factor equations under the same solver method are shown in every single plot.

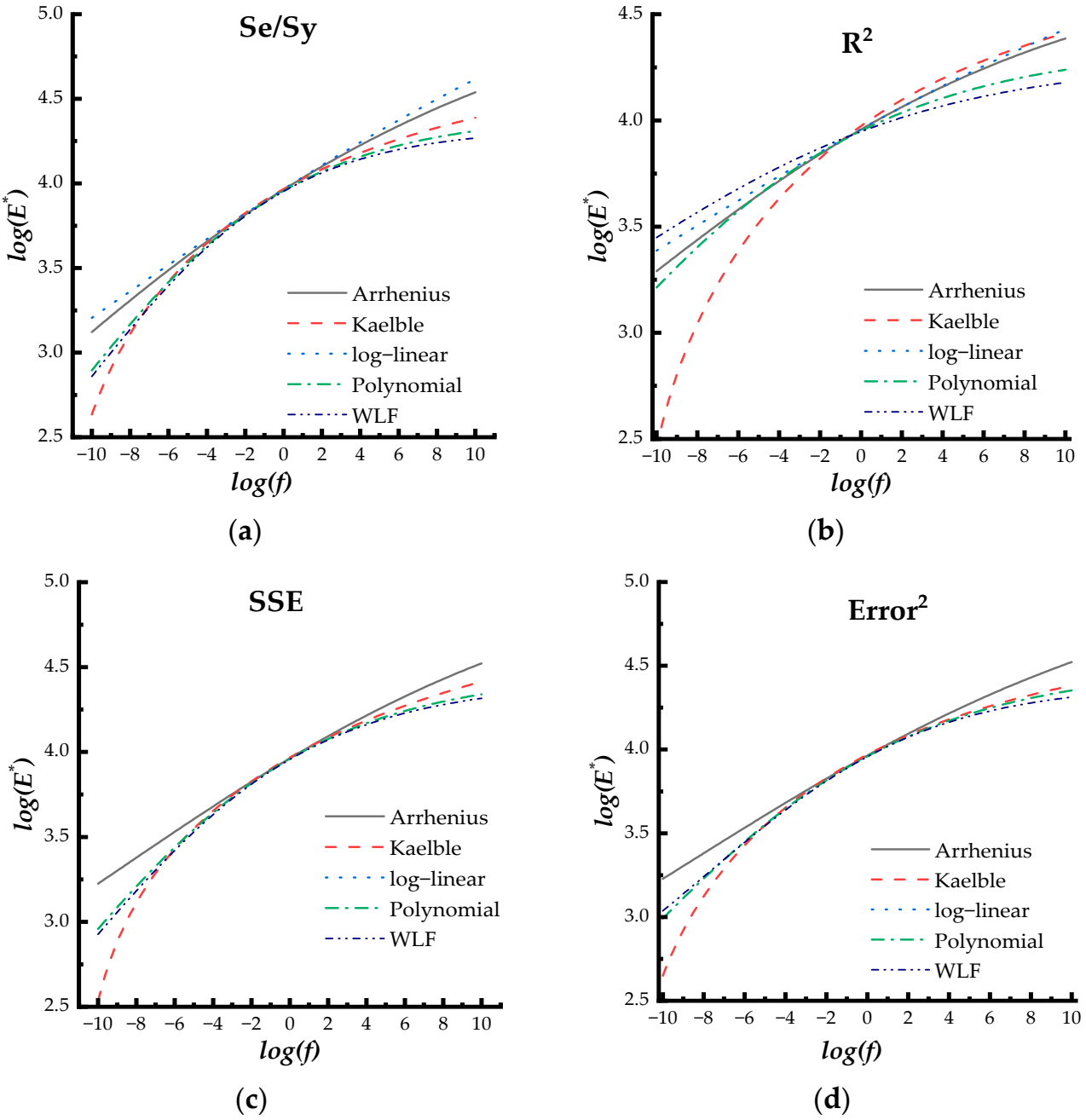


Figure 7. The master curve of GLS model fitting results with different shift factor equations. (**a**) Se/Sy minimization; (**b**) R^2 maximization; (**c**) SSE minimization; (**d**) $Error^2$ minimization.

3.2.3. The CAM Model Fitting Results Analysis

In Figure 8, the results of the CAM model's dynamic modulus master curve fitting are presented together with five shift factor equations utilizing four alternative solver methods. Under the same solver method, the fitting results of five different shift factor equations were plotted in a single plot to compare the effect of the solver method on different shift factor equations.

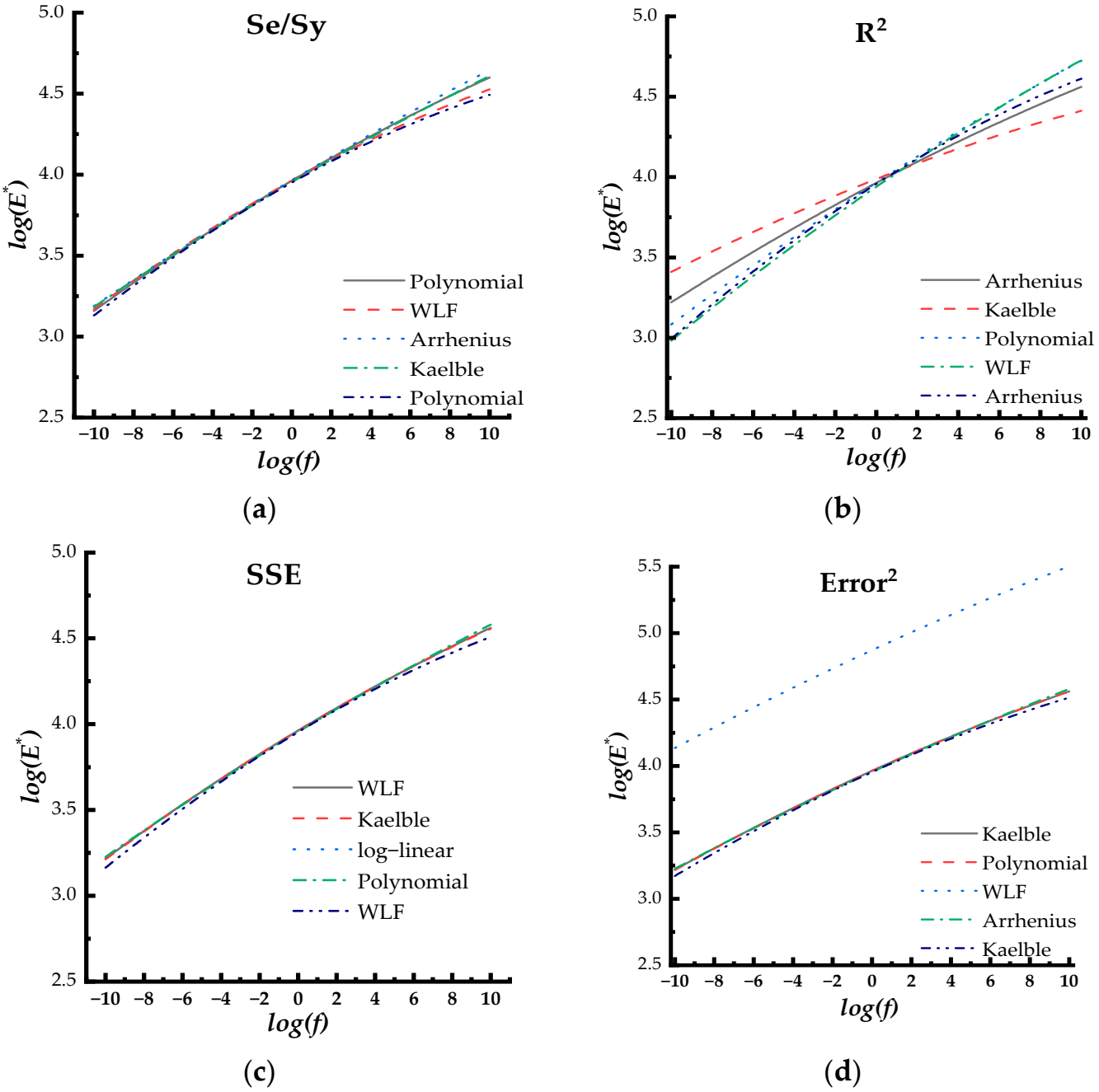


Figure 8. The master curve of CAM model fitting results with different shift factor equations. (**a**) Se/Sy minimization; (**b**) R^2 maximization; (**c**) SSE minimization; (**d**) $Error^2$ minimization.

3.2.4. The Modified CAM Model Fitting Results Analysis

Figure 9 shows the results of dynamic modulus master curve fitting using the modified CAM model along with four different solver methods and five distinct shift factor equations. For analyzing the effect of the solver method on different shift factor equations, the fitting results of different shift factor equations under the same solver method were plotted in a single picture.

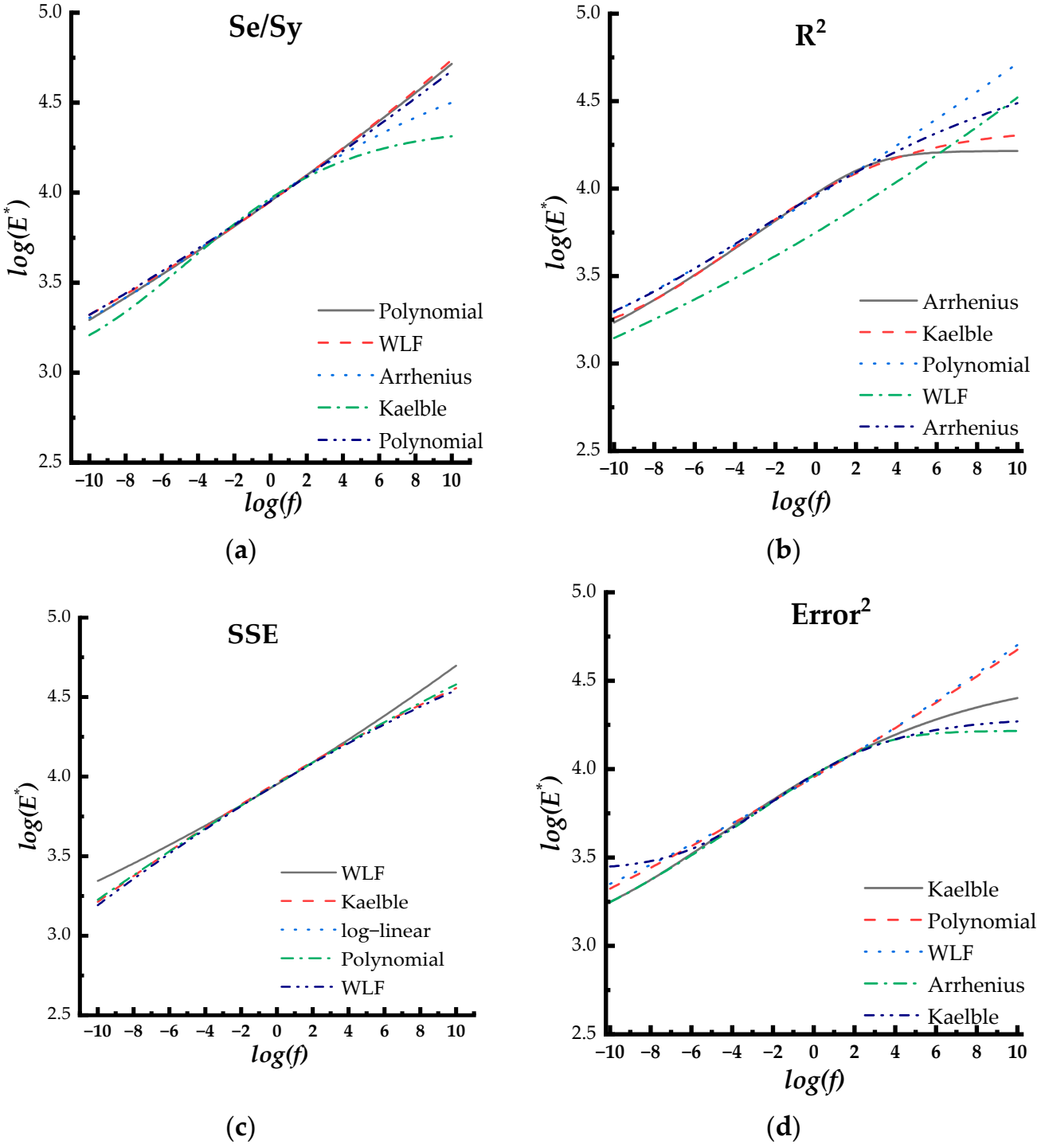


Figure 9. The master curve of modified CAM model fitting results with different shift factor equations. (**a**) Se/Sy minimization; (**b**) R^2 maximization; (**c**) SSE minimization; (**d**) $Error^2$ minimization.

3.2.5. The SCM Model Fitting Results Analysis

The dynamic modulus master curve fitting results of the SCM model along with five different shift factor equations under four solver methods were plotted in Figure 10. The fitting results under each solver method were shown in a single picture for comparing the effect of the solver method on different shift factor equations.

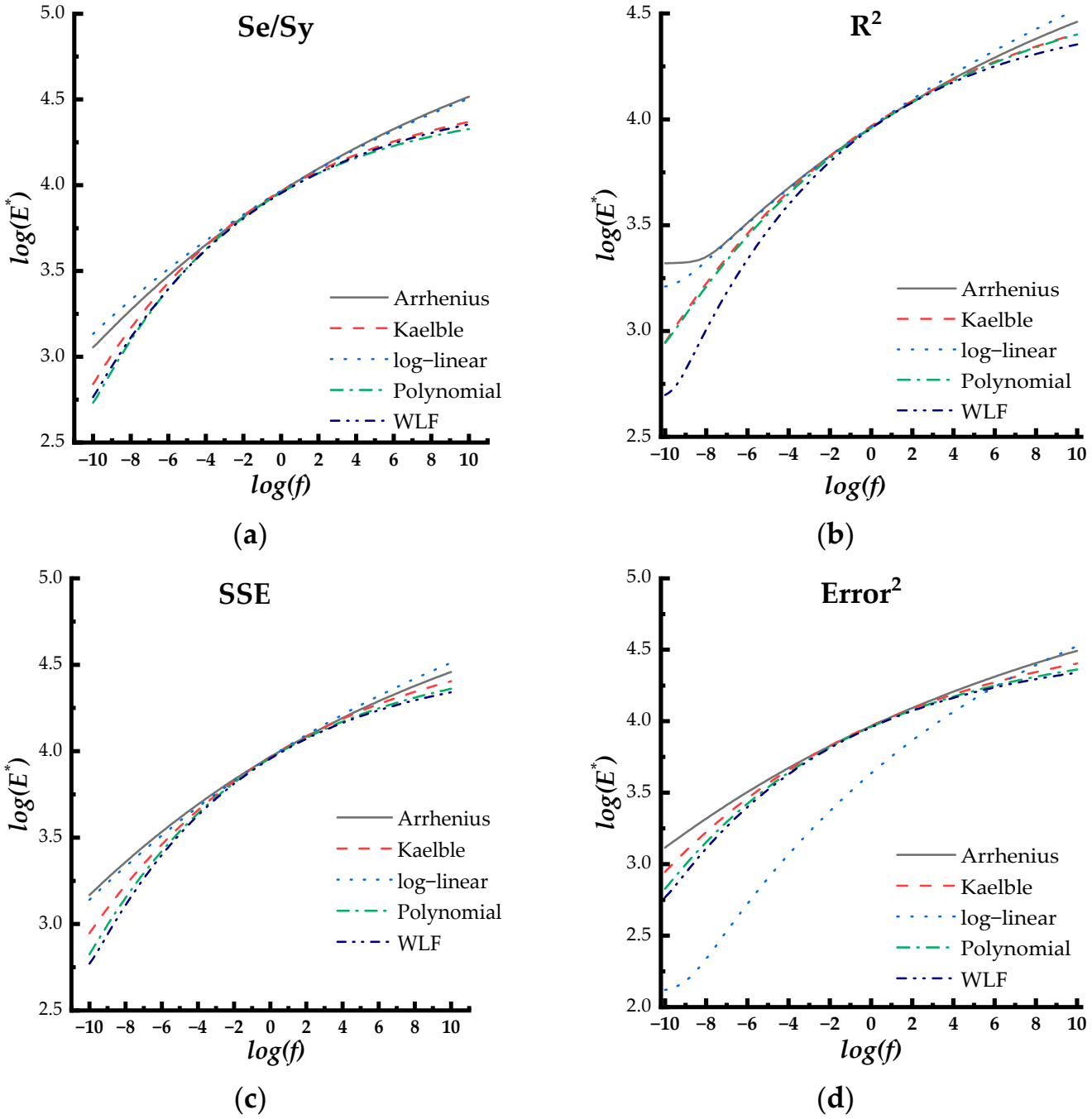


Figure 10. The master curve of SCM model fitting results with different shift factor equations. (**a**) Se/Sy minimization; (**b**) R^2 maximization; (**c**) SSE minimization; (**d**) $Error^2$ minimization.

3.3. Analyzing the Influence of Shift Factor Equation on the Fitting of Dynamic Modulus Master Curve

3.3.1. The SLS Model Fitting Results Analysis

The measured and predicted dynamic moduli fitted by the SLS model for different shift factor equations are compared in Figure 11. The linear fitting results of each shift factor equation were also obtained. In Figure 11, the red squares represent the spot of the predicted dynamic modulus by the SLS model corresponding to the measured dynamic modulus.

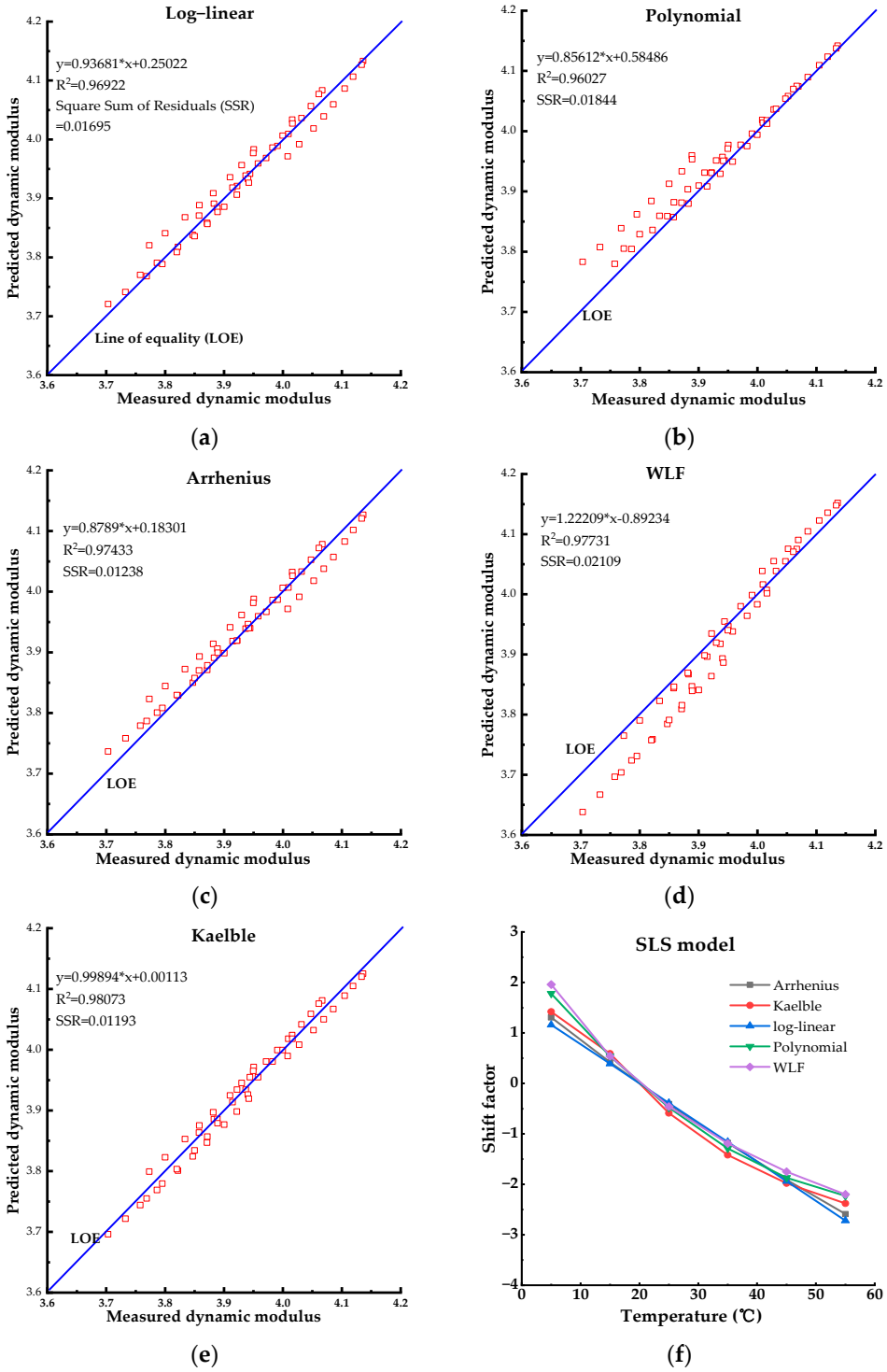


Figure 11. Comparison of predicted and measured dynamic modulus for different shift factor equations. (**a**) Log–linear equation; (**b**) Polynomial equation; (**c**) Arrhenius equation; (**d**) WLF equation; (**e**) Kaelble equation; (**f**) shift factors at different temperatures.

3.3.2. The GLS Model Fitting Results Analysis

Figure 12 showed the measured dynamic modulus versus the predicted dynamic modulus fitted by the GLS model for different shift factor equations. The line of equality (LOE) and linear fitting method were combined to compare the prediction accuracy of different shift factor equations. In Figure 12, the red squares represent the spot of the predicted dynamic modulus by the GLS model corresponding to the measured dynamic modulus.

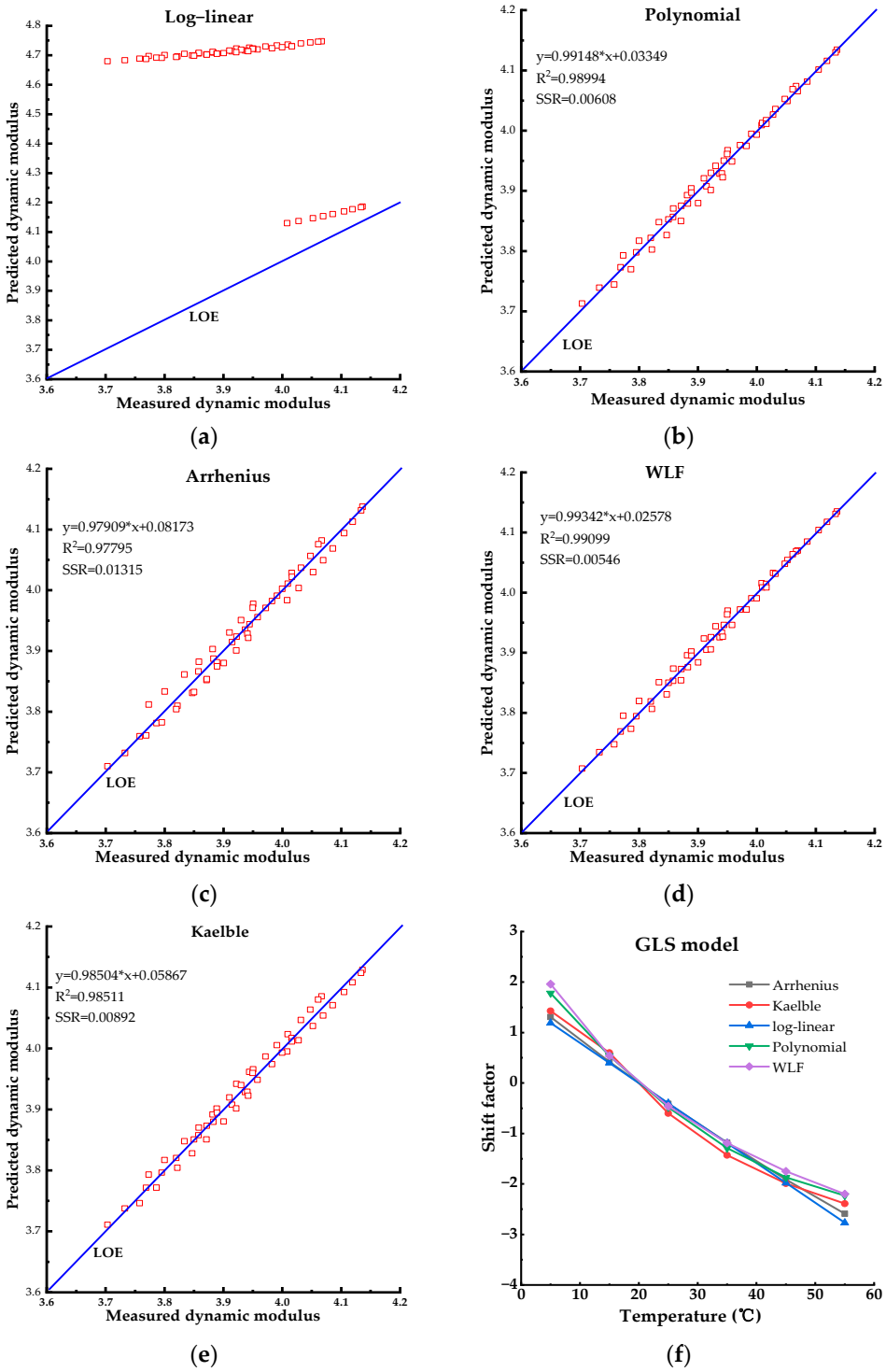


Figure 12. Comparison of predicted and measured dynamic modulus for different shift factor equations. (**a**) Log–linear equation; (**b**) Polynomial equation; (**c**) Arrhenius equation; (**d**) WLF equation; (**e**) Kaelble equation; (**f**) shift factors at different temperatures.

3.3.3. The CAM Model Fitting Results Analysis

Figure 13 compares the measured and predicted dynamic modulus fitted by the CAM model for different shift factor equations. For an accurate comparison, the LOT and linear fitting methods were adopted to compare the predicted and measured data. In Figure 13, the red squares represent the spot of the predicted dynamic modulus by the CAM model corresponding to the measured dynamic modulus.

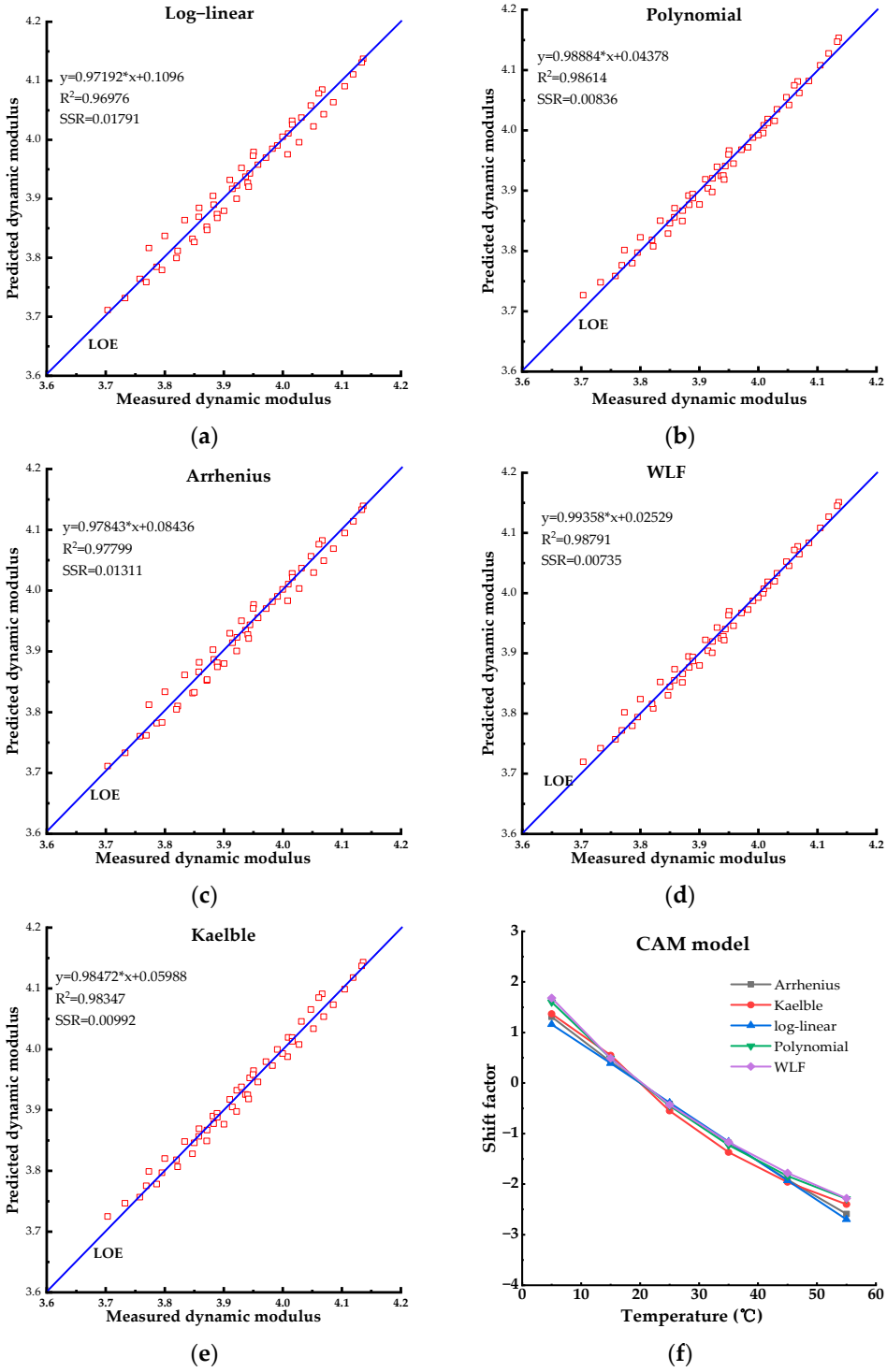


Figure 13. Comparison of predicted and measured dynamic modulus for different shift factor equations. (**a**) Log–linear equation; (**b**) Polynomial equation; (**c**) Arrhenius equation; (**d**) WLF equation; (**e**) Kaelble equation; (**f**) shift factors at different temperatures.

3.3.4. The Modified CAM Model Fitting Results Analyzing

Figure 14 gives the comparison between the measured and predicted dynamic modulus fitted by the modified CAM model for different shift factor equations. The LOE and linear fitting methods were used to analyze the prediction accurately. In Figure 14, the red squares represent the spot of the predicted dynamic modulus by the modified CAM model corresponding to the measured dynamic modulus.

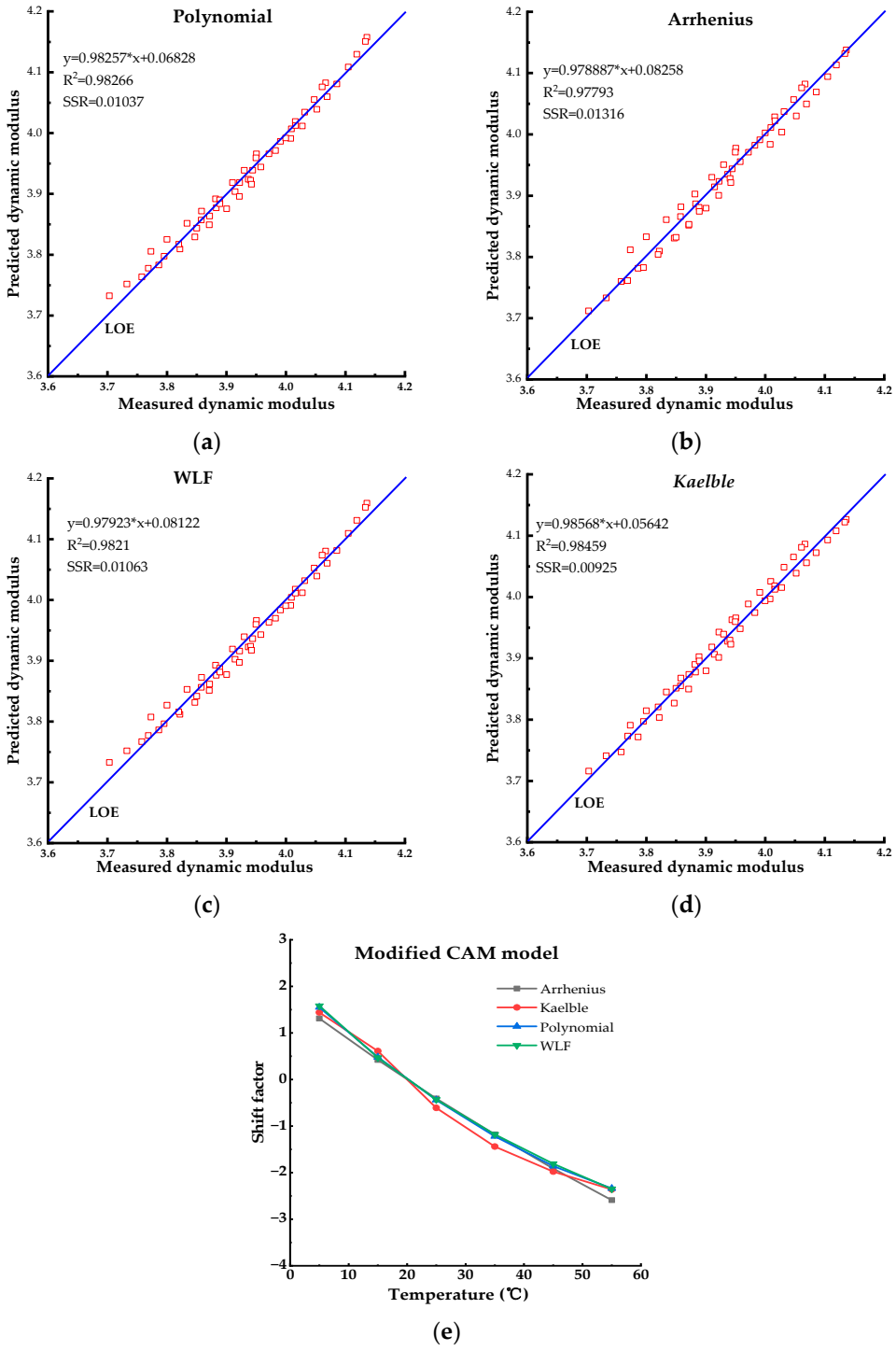


Figure 14. Comparison of predicted and measured dynamic modulus for different shift factor equations. (**a**) Polynomial equation; (**b**) Arrhenius equation; (**c**) WLF equation; (**d**) Kaelble equation; (**e**) shift factors at different temperatures.

3.3.5. The SCM Model Fitting Results Analysis

The comparison of the measured dynamic modulus was plotted against the predict–ed dynamic modulus fitted by the SCM model for different shift factor equations in Figure 15. The prediction accuracy was evaluated by the LOE and linear fitting methods. In Figure 15, the red squares represent the spot of the predicted dynamic modulus by the SCM model corresponding to the measured dynamic modulus.

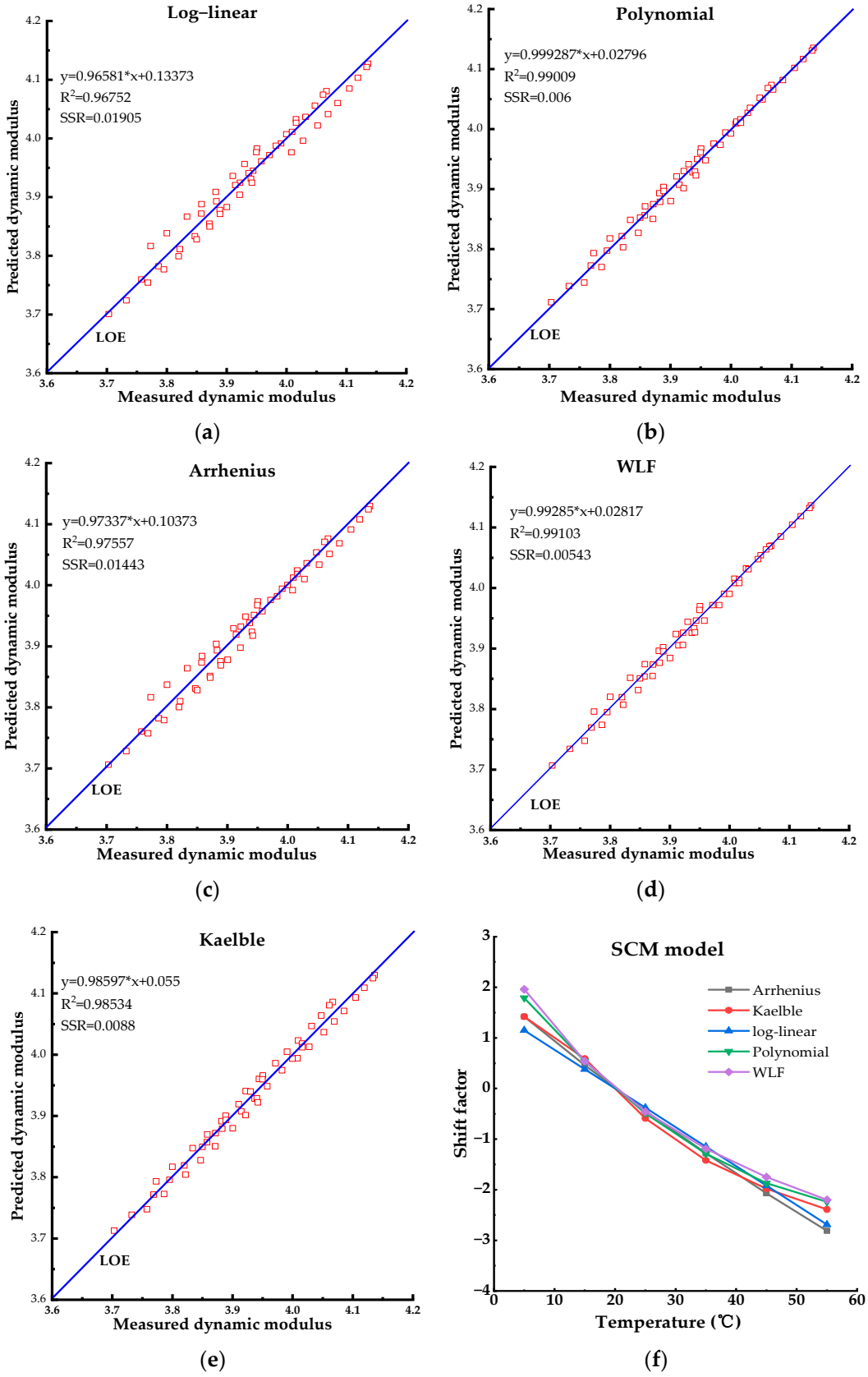


Figure 15. Comparison of predicted and measured dynamic modulus for different shift factor equations. (**a**) Log–linear equation; (**b**) Polynomial equation; (**c**) Arrhenius equation; (**d**) WLF equation; (**e**) Kaelble equation; (**f**) shift factors at different temperatures.

3.4. Comparing Master Curves with Recommended Models and Shift Factor Equations

3.4.1. Comparing the WLF Shift Factor Equation Fitting Results

In this section, the predicted dynamic modulus of different master curve models with the WLF shift factor equation is compared with the measured dynamic modulus in Figure 16. The prediction statistics results are organized in Table 1. According to the results of the analysis, the models with the highest prediction accuracy are recommended.

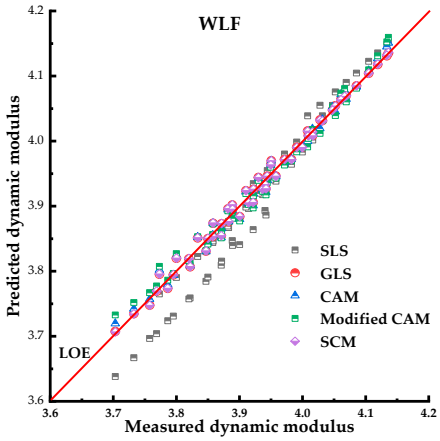


Figure 16. Comparison of predicted and measured dynamic modulus with different master curve models (WLF shift factor equation).

Table 1. The linear fitting results of different master curve models with the WLF shift factor equation.

Model	Fitting Equation	R^2	SSR
SLS	$Y = 1.22209 \times X - 0.89234$	0.97731	0.02109
GLS	$Y = 0.99342 \times X + 0.02578$	0.99099	0.00546
CAM	$Y = 0.99358 \times X + 0.02529$	0.98791	0.00735
Modified CAM	$Y = 0.97923 \times X + 0.08122$	0.9821	0.01063
SCM	$Y = 0.99285 \times X + 0.02817$	0.99103	0.00543

3.4.2. Comparing the Kaelble Shift Factor Equation Fitting Results

In this section, the predicted dynamic modulus of different master curve models with the Kaelble shift factor equation is compared with the measured dynamic modulus in Figure 17. The prediction statistics results are organized in Table 2. The models which had the highest prediction accuracy are recommended in the following section.

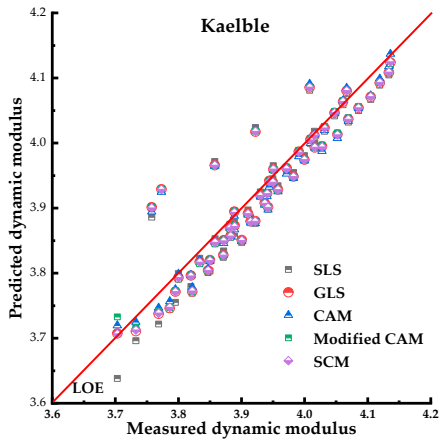


Figure 17. Comparison of predicted and measured dynamic modulus with different master curve models (Kaelble shift factor equation).

Table 2. The linear fitting results of different master curve models with the Kaelble shift factor equation.

Model	Fitting Equation	R^2	SSR
SLS	Y = 0.99894 × X + 0.00113	0.98073	0.01193
GLS	Y = 0.98504 × X + 0.05867	0.98511	0.00892
CAM	Y = 0.98472 × X + 0.05988	0.98347	0.00992
Modified CAM	Y = 0.98568 × X + 0.05642	0.98459	0.00925
SCM	Y = 0.98597 × X + 0.055	0.98534	0.0088

3.5. Comparing the Master Curves under Different Models

The master curves for different models with the WLF shift factor equation at the reference of 20 °C were plotted in Figure 18.

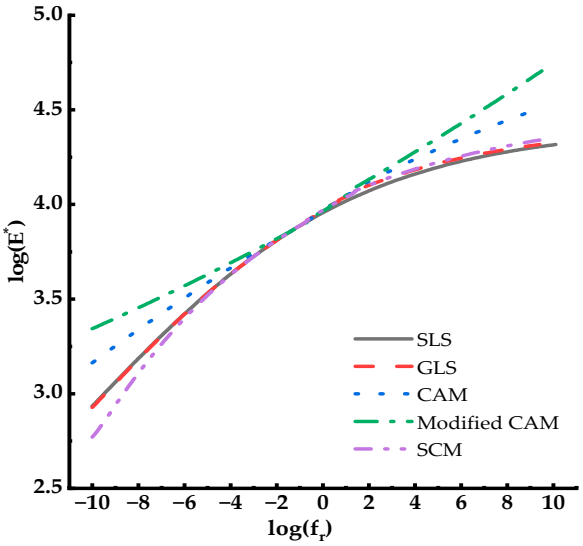


Figure 18. Master curve models of different models with WLF shift factor equation.

4. Discussion

4.1. Analyzing Master Curve Scale Type

From Figure 5b–d, it can be observed from the plots that the lines under different shift factor equations at low frequencies were close and difficult to distinguish when the loading frequency (f in Hz) and the dynamic modulus (E^* in MPa) were in arithmetical scale, or the dynamic modulus was in logarithmic scale and the loading frequency was in arithmetic scale. Hence, it was not suitable to compare the difference between different shift factor equations using these two scale types.

From Figure 5d, it can be noted that the lines under various shift factor equations at low frequency were closer than those at high frequency and closer than those in Figure 5a. Therefore, the log–log plots of dynamic modulus and loading frequency were adopted in this paper to illustrate the difference in dynamic modulus at lower frequencies and higher temperatures.

4.2. Analyzing the Influence of the Solver Method on the Fitting of the Dynamic Modulus Master Curve

4.2.1. The SLS Model Fitting Results Analysis

Observing the master curves plotted in Figure 6 indicated that there was scattering and variability in the master curves fitted by different solver methods. The scatter is minimal at a relatively intermediate frequency range. The master curve fitted by the SLS model combined with different shift factor equations and solver methods was similar at the intermediate frequency range (10^{-3}–10^{3} Hz), which was smaller than that of asphalt

mixtures [2]. When the loading frequency is higher than 10^3 Hz or lower than 10^{-3} Hz, the master curves exhibit some differences.

Based on the R^2 maximization solver method, the master curve of the Polynomial shift factor equation was different from others. For the $Error^2$ minimization solver method, the master curve of the log–linear shift factor equation was significantly higher than the others. Comparing the fitting results of four parameters (i.e., R^2, Se/Sy, $Error^2$, SSE values) calculated by four different solver methods, the fitting results calculated by the SSE and Se/Sy minimization solver methods were more accurate than the other two solver methods, i.e., the Se/Sy values calculated by the SSE and Se/Sy minimization solver methods were smaller than that of the R^2 maximization and $Error^2$ minimization solver methods. Therefore, the SSE and Se/Sy minimization solver methods are recommended for the SLS model for dynamic modulus master curve fitting.

4.2.2. The GLS Model Fitting Results Analysis

From Figure 7, the difference of dynamic modulus master curves fitted by various shift factor equations is not distinct at the intermediate frequency range. For the GLS model, when the R^2 maximization solver method was used, the master curve of the Kaelble shift factor equation differed from those fitted by the other three solver methods. It was difficult to use the shapes of master curves to distinguish the effect of solver methods. The fitting results (values of R^2, Se/Sy, $Error^2$, SSE) of the R^2 maximization solver method were relatively weaker than the other solver methods, i.e., the Se/Sy and $Error^2$ values of the R^2 maximization solver method were bigger than that of the other three methods. Therefore, the Se/Sy, SSE, and $Error^2$ solver methods are recommended for the GLS model for dynamic modulus master curve fitting.

4.2.3. The CAM Model Fitting Results Analysis

For the CAM model in Figure 8, when the R^2 maximization solver method was applied, the master curve of different shift factor equations had higher discreteness than the other solver methods. For the $Error^2$ minimization solver method, the master curve of the WLF shift factor equation was higher than the others. The master curves fitted by Se/Sy and SSE minimization solver methods were similar. At the same time, the fitting results (values of R^2, Se/Sy, $Error^2$, SSE) of the R^2 maximization and $Error^2$ minimization solver methods were not as good as the other two solver methods, i.e., the Se/Sy and $Error^2$ values of the R^2 maximization and $Error^2$ minimization solver methods were bigger than those of the other two solver methods. Therefore, the Se/Sy and SSE solver methods are recommended for the CAM model for dynamic modulus master curve fitting.

4.2.4. The Modified CAM Model Fitting Results Analysis

As shown in Figure 9, when the R^2 maximization, $Error^2$, and Sy/Sy minimization solver methods were used for the modified CAM model, the master curve of different shift factor equations had higher discreteness than the SSE minimization solver method. The parameters fitted by four different solver methods would also prove the results above, e.g., the R^2 value of the SSE minimization solver method was bigger than the other three solver methods and the Sy/Sy value of the SSE minimization solver method was smaller than the other three solver methods. Therefore, the SSE minimization solver method is recommended for the modified CAM model for dynamic modulus master curve fitting.

4.2.5. The SCM Model Fitting Results Analyzing

When the R^2 maximization and $Error^2$ minimization solver methods were utilized, the master curve of different shift factor equations had higher discreteness than the other solver methods for the SCM model in Figure 10. These results could also be proven by the parameter values (i.e., R^2, Se/Sy, $Error^2$, SSE values); the Se/Sy and SSE values of the SSE and Se/Sy minimization solver methods were smaller than that of the other two solver methods. Therefore, the SSE and Se/Sy minimization solver methods are recom-

mended for the SCM model for dynamic modulus master curve fitting by graphical and statistical comparison.

Based on the graphical comparison and statistical analysis of the fitting results of four solver methods under different master curve models and shift factor equations, the recommended solver method is that the SSE minimization ($\leq$0.02) should be used as the solver method, the solver methods of Se/Sy ($\leq$0.02) and Error^2 ($\leq$0.02) minimization, and R^2 maximization ($\geq$0.99) could be used as the added bounds. This combination would produce the optimum master curve fitting results for all master curve models.

4.3. Analyzing the Influence of Shift Factor Equation on the Fitting of Dynamic Modulus Master Curve

4.3.1. The SLS Model Fitting Results Analysis

The line of equality methods and trend line statistics, i.e., trend line R^2 and trend line slope, were employed to statistically evaluate the accuracy of the model in determining predicted results from measured results. The trend line slope values higher than one and lower than one represent over–estimation and underestimation of the dynamic modulus.

An indicator of the overall bias of a prediction model is how closely its unconstrained linear trend line matches the line of equality (LOE). The prediction is more precise the closer the data point is to the LOE. In other words, it indicates how the unconstrained intercept and slope are quite close to 0 and 1, respectively. The bias will be lower [62,66,67] the closer the intercept is to zero and the slope is to unity. The slope of the linear relationship between predicted and measured results with the intercept set close to zero was used to evaluate the deviation of the model's predictions from the measured values. The R^2 value of the linear relationships provides information about the variability of the predicted results explained by each model, and it can be used to indicate the overall accuracy of the model. The degree of correlation between predicted and measured results increased as the R^2 value approached 1.

According to Figure 11, the SLS model with different shift factor equations generally produced prediction results that were close to the measured results, and a relatively good correlation was discovered between measured and predicted results. However, the prediction accuracy varied with shift factor equations. It showed that based on the trend line R^2 values, the fitting accuracy of different shift factor equations was ranked as Polynomial < log–linear < Arrhenius < WLF < Kaelble and the trend line R^2 values increased from 0.96027 to 0.98073. The Kaelble shift factor equation had the strongest R^2 value and showed the best goodness–of–fit statistics for the SLS model, which was able to predict the dynamic modulus that was more accurately matched with the measured values. This result may be explained by the equation form of the Kaelble shift factor equation, which had two regression parameters and the most complicated equation form. The data generated by the Kaelble shift factor equation were generally distributed along the line of equality (LOE), which also confirmed the conclusion. The trend line slope of the Kaelble shift factor equation was closer to one than the other shift factor equations, and all the trend line slopes of different shift factor equations were somewhat smaller than one, indicating that the SLS model with different shift factor equations would underestimate the measured dynamic modulus.

The shift factors for different shift factor equations at different temperatures are presented in Figure 11f. It was observed from the plot that the shift factors changed slightly at high or low temperatures, and the shift factor equations had relatively little influence on the shift factor values.

Statistical analysis was performed to examine the accuracy of the predicted dynamic modulus predicted by different master curve models and shift factor equations. The Pearson linear correlation analysis was introduced for comparing the correlation between the measured and predicted dynamic modulus. If the *p*-value is less than 0.01 (i.e., significance level), the two compared groups are statistically equivalent; otherwise, they can be assumed to be statistically different. According to the relevant research results, the smaller the *p*-value,

the better the fitting effect and the more credible the regression equation. When *p*-value < 0.01, there is a very significant correlation between predicted and measured results. According to the SPSS analysis, the *p*-values of all five shift factor equations were all smaller than 0.01. Hence, there is a statistically acceptable correlation between the measured and predicted dynamic modulus at a 99% significance level. The Kaelble shift factor equation had the highest Pearson correlation index.

According to the statistical and graphical analysis, the Kaelble shift factor equation for the SLS model was able to predict the dynamic modulus most accurately with the highest trend line R^2 value and Pearson correlation index.

4.3.2. The GLS Model Fitting Results Analysis

The spots fitted by the log–linear shift factor equation were away from the LOE, so the log–linear shift factor equation was not suitable for the GLS model. Excluding the log–linear shift factor equation, it was found that the fitting accuracy of different shift factor equations was ranked as Arrhenius < Kaelble < Polynomial < WLF based on the trend line R^2 values, and the trend line R^2 values increased from 0.97795 to 0.99099. According to the goodness–of–fit ranking criteria, the fitting results of R^2 values showed that all four equations considered fit the data satisfactorily. For the GLS model, the WLF shift factor equation showed the best agreement between predicted and measured results and was able to predict dynamic modulus more precisely. The data spots generated by the WLF shift factor equation were clustered tightly along the LOE as shown in Figure 12d. The WLF shift factor equation displayed a slope close to 1 (0.99342) as compared to the other shift factor equations, and all the trend line slopes of different shift factor equations were slightly smaller than 1, which means that the GLS model with different shift factor equations would underestimate the measured dynamic modulus. It could be found from Figure 12f that the shift factors for different shift equations at different temperatures exhibited a pattern of regularity similar to that of the SLS model. For the GLS model, the shift factor equations had an insignificant influence on the shift factor values.

According to the Pearson linear correlation analysis, the *p*-values of all four shift factor equations (except the log–linear shift factor equation) were all smaller than 0.01. Therefore, there was a statically good correlation between the measured and predicted dynamic modulus at a 99 % significance level. The WLF shift factor equation had the highest Pearson correlation index. Therefore, according to the statistical and graphical analysis of the comparing results of the GLS model with different shift factor equations, the WLF shift factor equation for the GLS model was able to predict the dynamic modulus most accurately with the highest trend line R^2 value and Pearson correlation index.

4.3.3. The CAM Model Fitting Results Analysis

As observed in Figure 13, the trend line R^2 values of different shift factor equations increased from 0.96976 to 0.98791, and the fitting accuracy for all shift factor equations was ranked as log–linear < Arrhenius < Kaelble < Polynomial < WLF based on the trend line R^2 values. The WLF shift factor equation had the strongest R^2 value for the CAM model, indicating a high–level explanation for the variability among measured dynamic modulus. The scatter among the data generated by the WLF shift factor equation was less insignificant than that produced by the other equations. The trend line slope of the WLF shift factor equation was closer to one than that of the other shift factor equations, and all the trend line slopes of different shift factor equations were slightly smaller than one, which means that the CAM model with all shift factor equations would underestimate the measured dynamic modulus. The shift factors for different shift factor equations at different temperatures are represented in Figure 13f. It was observed from the plot that the shift factors exhibited higher variation at high or low temperatures and less variation at intermediate temperatures. Therefore, the shift factor equations were able to influence the shift factor values more significantly at high or low temperatures.

Based on the Pearson linear correlation analysis results, the *p*-values of each of the five shift factor equations were all smaller than 0.01. Therefore, there was a statically good correlation between measured and predicted dynamic modulus at a 99% significance level. The WLF shift factor equation had the highest correlation index. Therefore, according to the statistical and graphical analysis of the comparing results of the CAM model with different shift factor equations, the WLF shift factor equation for the CAM model was able to predict the dynamic modulus most accurately with the highest trend line R^2 value and Pearson correlation index.

4.3.4. The Modified CAM Model Fitting Results Analysis

When the log–linear shift factor equation was used in the modified CAM model, there were no appropriate fitting results. From Figure 14, the fitting accuracy of different shift factor equations for the modified CAM model was ranked as Arrhenius < WLF < Polynomial < Kaelble based on the trend line R^2 values. The trend line R^2 values increased from 0.97793 to 0.98459. The Kaelble shift factor equation demonstrated the best goodness–of–fit statistics for the modified CAM model and was able to predict dynamic modulus more accurately in comparison to the measured values. The data spots generated by the Kaelble shift factor equation were generally distributed along the LOE. All the trend line slopes of different shift factor equations were slightly smaller than one, and the Kaelble shift factor equation's slope was closer to one than those of the other shift factor equations. This indicated that the modified CAM model with different shift factor equations would underestimate the measured dynamic modulus. From Figure 14e, the shift factors at various temperatures showed very little variation, therefore, the shift factor equations had little effect on the shift factor values for the modified CAM model.

According to the Pearson linear correlation analysis, the *p*-values of the four shift factor equations were all smaller than 0.01. Therefore, there was a statistically good correlation between the measured and predicted dynamic modulus at a 99% significance level. The Kaelble shift factor equation had the highest correlation index. Therefore, according to the statistical and graphical analysis of the comparing results of the modified CAM model with different shift factor equations, the Kaelble shift factor equation for the modified CAM model was able to predict the dynamic modulus most accurately with the highest trend line R^2 value and Pearson correlation index.

4.3.5. The SCM Model Fitting Results Analyzing

From Figure 15, it can be seen that the fitting accuracy of different shift factor equations was ranked as log–linear < Arrhenius < Kaelble < Polynomial < WLF based on the trend line R^2 values. The prediction R^2 values dramatically improved from 0.96752 to 0.99103. For the SCM model, the WLF shift factor equation showed the best goodness–of–fit statistics and was able to predict dynamic modulus more accurately. The WLF shift factor equation demonstrated the best goodness–of–fit. The data spots generated by the WLF shift factor equation were well linearly distributed along the LOE. Compared to the other shift factor equations, the trend line slope of the WLF shift factor equation was closer to one and showed improved accuracy. All the trend–line slopes of different shift factor equations were slightly smaller than one, demonstrating that the measured dynamic modulus would be underestimated by the SCM model with shift factor equations. The shift factors for different shift equations at different temperatures showed a pattern of regularity resembling that of the SLS model. The same conclusion could be drawn that the shift factor equations had little influence on the shift factor values for the SCM model.

The *p*-values of all five shift factor equations were all smaller than 0.01 according to the Pearson linear correlation analysis. Hence, there was a statically good correlation between measured and predicted dynamic modulus at a 99% significance level. The WLF shift factor equation had the highest correlation index. Therefore, according to the statistical and graphical analysis of the comparing results of the SCM model with different shift factor equations, the WLF shift factor equation for the SCM model was able to predict

the dynamic modulus most accurately with the highest trend line R^2 value and Pearson correlation index.

Based on the statistical and graphical analysis above, the WLF and Kaelble shift factor equation, which indicated excellent goodness–of–fit and had a greater degree of freedom, are recommended for shifting the dynamic modulus at different test temperatures and obtaining the dynamic modulus master curves. This finding was consistent with the conclusion in reference [29] and different from the conclusion in reference [33]. The trend line, LOE, and Pearson linear correlation analysis proved to be effective ways to analyze the fitting results of different master curve models with different shift factor equations.

4.4. Comparing Master Curves with Recommended Models and Shift Factor Equations

4.4.1. Comparing the WLF Shift Factor Equation Fitting Results

It was discovered from Figure 16 and Table 1 that the spots predicted by the SLS model were located away from the LOE, and the trend line R^2 value of the SLS model linear fitting was the smallest, the slope was much larger than 1. The GLS and SCM model had almost identical fitting results, e.g., the trend line R^2 values were 0.99099 and 0.99103, and the SSR values were 0.00546 and 0.00543 respectively. At the same time, the slopes were 0.99342 and 0.99285. Therefore, the GLS and SCM models had better goodness–of–fit than the other models, and so the GLS and SCM models can characterize the asymmetry of the dynamic modulus master curve. This finding was in line with the literature [29,68].

The R^2 values of models used for PU mixtures were much higher than that for asphalt mixtures, for example, in reference [69], the R^2 values ranged from 0.851 to 0.858 for SLS, GLS, and SCM models. Therefore, the SLS model exhibited the worst–fit statistic, and the dynamic modulus values predicted by the GLS and SCM models appeared to fit the measured data better than the ones predicted by the other models.

4.4.2. Comparing the Kaelble Shift Factor Equation Fitting Results

It was observed from Figure 17 and Table 2 that the spots predicted by the SLS and SCM models were distant from the LOE. The R^2 value and slope of different model linear fittings were close, the trend line R^2 values of all models were all slightly higher than 0.98, and the SLS model had the smallest trend line R^2 value and the highest SSR value. The slope of the SLS model was closer to 1; at the same time, the slopes of the other models were similar and slightly smaller than that of the SLS model. As a result, different master curve models exhibited similar fitting results, and the fitting results had a slight difference, and the fitting results, e.g., trend line R^2 value and trend line slopes, were smaller than those of the WLF shift factor equation.

According to the statistical and graphical analysis of the comparing results, the WLF shift factor equation in conjunction with the GLS and SCM models showed the best accuracy of prediction for the dynamic modulus of PU mixtures. The fact that the GLS and SCM models have more parameter freedoms than the other models may help to explain this.

4.5. Comparing the Master Curves under Different Models

Based on visual inspection of the plots, it can also be learned from Figure 18 that the CAM and modified CAM models were found to have greater dynamic modulus values than the SLS, GLS, and SCM models at a high and low frequency based on visual examination of the plots. The master curve of the SCM model was lower than the master curves of the SLS and GLS models at a lower loading frequency (10^{-5} Hz), the SLS and GLS model were in good agreement. This phenomenon could be explained by the fact that the loading frequency range in the dynamic modulus test was narrower (only from 25 Hz to 0.1 Hz, or 1.398 to −1 in log form) compared with the frequency of the master curve. Therefore, it was difficult to tell the difference between the master curves of the SLS and GLS models during the loading frequency range. The shape of the SLS model was similar to the results of the dense PU mixture in [54].

The dynamic modulus master curve of the PU mixture did not follow the traditional smooth "S" shape commonly reported in [70] and did not flatten out at higher or lower frequency as much as the master curve of asphalt mixture fitted by the SLS, GLS, and SCM models [32,71]. The "S" shape of the asphalt mixture dynamic modulus master curve could reflect the mechanical properties of the full loading frequency range. For the asphalt mixture, the dynamic modulus would tend to be limited when the loading frequency is low enough or high enough [72,73], and this feature is very important for the viscoelastic property of the asphalt mixture. The "S" shape of the asphalt mixture dynamic modulus master curve means that the asphalt mixture would exhibit elastic properties at higher frequency (or low temperature) but exhibit viscous properties at a lower frequency (or high temperature). The dynamic modulus of the PU mixture did not present the ultimate dynamic modulus at high or low loading frequency; this phenomenon was not consistent with the findings in the literature [32]. All five models in the literature [32] reached a low–temperature threshold for the dynamic modulus of the asphalt mixture when considering the asymptotic limits.

The ultimate dynamic modulus of the asphalt mixture is only related to the mixture gradation, which depends on the volume characteristic [42,74]. It is important to research both the ultimate dynamic modulus and the critical factors which could determine the ultimate dynamic modulus. Asphalt is considered the source of the viscoelasticity of the asphalt mixture [75]. Therefore, the dynamic modulus is the intrinsic material property of the PU mixture [54], and the viscoelastic property of the PU mixture is different from that of the asphalt mixture.

5. Conclusions

This paper focused on the dynamic modulus master curve of a PU mixture with dense gradation. To fit the dynamic modulus master curve, five master curve models including the SLS, GLS, CAM, modified CAM, and SCM models and five shift factors i.e., the log–linear, Arrhenius, Kaelble, Polynomial, and WLF equations were combined. The parameters of the master curve and shift factor equations were obtained through the regression process by using four kinds of error minimization methods, i.e., the solver method. The effect of various models, shift factors, and solver method combinations on the goodness–of–fit statistics was examined and compared in this study. According to the discussion, the following recommendations for the model, shift factor, and solver method combination with the best prediction accuracy of dynamic modulus were made:

(1) By comparing the log–log plot, arithmetic plot, and semi–log plot results, it was found that the log–log plot clearly showed the difference between different dynamic modulus curves at low and high loading frequencies. It is recommended for fitting the dynamic modulus master curve and the analysis of the dynamic modulus of the PU mixture.

(2) Different solver methods generate different master curves; by comparing fitting results (i.e, R^2, Se/Sy, $Error^2$, and SSE values) of the master curves constructed by different shift factor equations under different solver methods, the SSE and Se/Sy minimization solver methods are suggested for the SLS, CAM, and SCM model; the Se/Sy, SSE, and $Error^2$ minimization solver methods are proposed for the GLS model; the SSE minimization solver methods are recommended for the modified CAM model.

(3) The SSE minimization solver method is recommended as the solver method, which could be set as $\leq$0.02; the Se/Sy minimization ($\leq$0.02) and $Error^2$ minimization ($\leq$0.02), and R^2 maximization ($\geq$0.99) were used as the added bound. This proved to be the most accurate solver method for the dynamic modulus master curve fitting.

(4) The accuracy between the measured results and the predicted results that were regressed by the SSE minimization solver method could be statistically analyzed using the line of equality methods and trend line statistics.

(5) For five master curve models, the *p*-value of the Pearson linear correlation analysis proved that the measured results had a significant correlation with the predicted results for

five shift factor equations. However, the log–linear shift factor equation failed to provide satisfactory fitting results in the GLS and modified CAM models.

(6) For the SLS and modified CAM models, the trend line R^2 values increased from 0.96027 to 0.98073, from 0.96752 to 0.99103, respectively; the Kaelble shift factor equation had the strongest trend line R^2 values, and its trend line slope was closer to 1.

(7) For the GLS, CAM, and SCM models, the trend line R^2 values increased from 0.97795 to 0.99099, from 0.96976 to 0.98791, and from 0.96752 to 0.99103, respectively. The WLF shift factor equation had the highest trend line R^2 values, and its trend line slope was closer to 1.

(8) The GLS and SCM models combined with the WLF shift factor equation showed the greatest predictive accuracy for PU mixture dynamic modulus.

(9) The shape of the dynamic modulus master curve of the PU mixture did not follow the traditional smooth "S" shape as shown in the asphalt mixture; the master curve of the PU mixture did not flatten out at high or low frequency. The viscoelasticity of the PU mixture is different from that of the asphalt mixture.

The study determined the best axis plot form, solver method, shift factor equation, and master curve model for the dynamic modulus master curve of the PU mixture, and the dynamic modulus master curves of the PU mixture were constructed and compared with that of the asphalt mixture. It has been established that the viscoelasticity of the PU mixture was proved to be different from the asphalt mixture. This paper provides fundamental study and information about the dynamic modulus master curve and the viscoelastic property of the PU mixture. The results of this study supply information for the dynamic modulus of the PU mixture when the pavement structure consists of PU mixture layers and could help to ascertain the optimum pavement layer thickness which could resist permanent deformation at higher temperatures. This study also makes it possible to design a pavement structure with the parameters at a higher temperature instead of parameters at 15 °C which is used in the current pavement structure design procedure; this change could improve the accuracy of pavement structure design. There were no studies into the suitable dynamic modulus master curve mathematical equation for the PU mixture; the innovation of this paper was to determine the suitable master curve models for the PU mixture and partially fill the gap in the dynamic mechanical study of the PU mixture.

This paper only studied and compared the dynamic modulus of the PU mixture with dense gradation; the factors that may influence the dynamic modulus of the PU mixture, e.g., aggregate gradation, aggregate type, and PU content, need to be studied and analyzed in future research. In addition, it is important to study the ultimate dynamic modulus of the PU mixture which is related to the viscoelasticity of the PU mixture. In this paper, only five traditional mathematical equations introduced from the asphalt mixture master curve construction were compared and analyzed for the applicability of the equations for the dynamic modulus master curve of the PU mixture. This is only the first step in analyzing the dynamic modulus master curve of the PU mixture. The study of the dynamic modulus of the PU mixture is a complicated systematic work, and the next stop should be to use the neural network methods to develop new mathematical equations which are more suitable for the dynamic modulus master curve of the PU mixture.

Author Contributions: Conceptualization, H.Z.; methodology, S.M. and B.M.; software, W.G.; validation, H.Z., W.G. and J.W.; formal analysis, H.Z.; investigation, H.Z. and S.C.; resources, W.G., W.Z., B.M. and F.L.; data curation, H.Z., S.C., B.M., F.L. and S.L.; writing—original draft preparation, H.Z.; writing—review and editing, S.M.; visualization, H.Z., S.C., C.S. and J.W.; supervision, S.M.; project administration, W.Z. and S.M.; funding acquisition, W.Z. All authors have read and agreed to the published version of the manuscript.

Funding: This research received no external funding.

Institutional Review Board Statement: Not applicable.

Informed Consent Statement: Not applicable.

Data Availability Statement: The data that support the findings of this study are available on request from the corresponding author, Shijie M, upon reasonable request.

Acknowledgments: We thank Guang Li, and Peiyu Zhang for their assistance with experiments and valuable discussion.

Conflicts of Interest: The authors declare no conflict of interest.

References

1. Christensen, D. Analysis of creep data from indirect tension test on asphalt concrete. *J. Assoc. Asph. Paving Technol.* **1998**, *67*, 458–492.
2. Lee, H.-J.; Kim, Y.R. Viscoelastic Constitutive Model for Asphalt Concrete under Cyclic Loading. *J. Eng. Mech.* **1998**, *124*, 32–40. [CrossRef]
3. Gibson, N.H.; Schwartz, C.W.; Schapery, R.A.; Witczak, M.W. Viscoelastic, Viscoplastic, and Damage Modeling of Asphalt Concrete in Unconfined Compression. *Transp. Res. Rec. J. Transp. Res. Board* **2003**, *1860*, 3–15. [CrossRef]
4. Diab, A.; You, Z.; Adhikari, S.; Li, X. Modeling shear stress response of bituminous materials under small and large strains. *Constr. Build. Mater.* **2020**, *252*, 119133. [CrossRef]
5. Nguyen, Q.T.; Di Benedetto, H.; Sauzéat, C. Linear and nonlinear viscoelastic behaviour of bituminous mixtures. *Mater. Struct.* **2014**, *48*, 2339–2351. [CrossRef]
6. Zhang, F.; Hu, C.; Zhuang, W. The research for low-temperature rheological properties and structural characteristics of high-viscosity modified asphalt. *J. Therm. Anal. Calorim.* **2017**, *131*, 1025–1034. [CrossRef]
7. Venudharan, V.; Biligiri, K.P.; Das, N.C. Investigations on behavioral characteristics of asphalt binder with crumb rubber modification: Rheological and thermo−chemical approach. *Constr. Build. Mater.* **2018**, *181*, 455–464. [CrossRef]
8. Nemati, R.; Dave, E.V. Nominal property based predictive models for asphalt mixture complex modulus (dynamic modulus and phase angle). *Constr. Build. Mater.* **2018**, *158*, 308–319. [CrossRef]
9. Podolsky, J.H.; Williams, R.C.; Cochran, E. Effect of corn and soybean oil derived additives on polymer-modified HMA and WMA master curve construction and dynamic modulus performance. *Int. J. Pavement Res. Technol.* **2018**, *11*, 541–552. [CrossRef]
10. Badeli, S.; Carter, A.; Doré, G. Effect of laboratory compaction on the viscoelastic characteristics of an asphalt mix before and after rapid freeze-thaw cycles. *Cold Reg. Sci. Technol.* **2018**, *146*, 98–109. [CrossRef]
11. Christensen, D.W.; Anderson, D.A. Interpretation of dynamic mechanical test data for paving grade asphalt cements (with discussion). *J. Assoc. Asph. Paving Technol.* **1992**, *61*, 67–116.
12. Schwartz, C.W.; Gibson, N.; Schapery, R.A. Time-Temperature Superposition for Asphalt Concrete at Large Compressive Strains. *Transp. Res. Rec. J. Transp. Res. Board* **2002**, *1789*, 101–112. [CrossRef]
13. Chehab, G.; Kim, Y.-R.; Schapery, R.; Witczak, M.W.; Bonaquist, R. Time-temperature superposition principle for asphalt concrete with growing damage in tension state. *J. Assoc. Asph. Paving Technol.* **2002**, *71*, 559–593.
14. Witczak, M.W. *Simple Performance Test for Superpave Mix Design*; Transportation Research Board: Washington, DC, USA, 2002; Volume 465.
15. Airey, G.D. Use of black diagrams to identify inconsistencies in rheological data. *Road Mater. Pavement Des.* **2002**, *3*, 403–424. [CrossRef]
16. Kim, Y.R.; Lee, Y.-C. Interrelationships among stiffnesses of asphalt aggregate mixtures. *Asph. Paving Technol.* **1995**, *64*, 575–610.
17. Olard, F.; Di Benedetto, H. General "2S2P1D" Model and Relation Between the Linear Viscoelastic Behaviours of Bituminous Binders and Mixes. *Road Mater. Pavement Des.* **2011**, *4*, 185–224. [CrossRef]
18. Pellinen, T.; Witczak, M.; Bonaquist, R. Asphalt Mix Master Curve Construction Using Sigmoidal Fitting Function with Non-Linear Least Squares Optimization. In *Recent Advances in Materials Characterization and Modeling of Pavement Systems*; Columbia University: New York, NY, USA, 2004; pp. 83–101.
19. Sirin, O.; Paul, D.K.; Khan, M.S.; Kassem, E.; Darabi, M.K. Effect of Aging on Viscoelastic Properties of Asphalt Mixtures. *J. Transp. Eng. Part B Pavements* **2019**, *145*, 04019034. [CrossRef]
20. Weibull, W. A statistical distribution function of wide applicability. *J. Appl. Mech.* **1951**, *18*, 293–297. [CrossRef]
21. Marasteanu, M.; Anderson, D. Improved model for bitumen rheological characterization. In Proceedings of the Eurobitume Workshop on Performance Related Properties for Bituminous Binders, Brussels, Belgium, May 1999.
22. Havriliak, S.; Negami, S. A complex plane analysis of α-dispersions in some polymer systems. *J. Polym. Sci. Part C Polym. Symp.* **1966**, *14*, 99–117. [CrossRef]
23. Yusoff, N.I.M.; Mounier, D.; Marc-Stéphane, G.; Hainin, M.R.; Airey, G.D.; Di Benedetto, H. Modelling the rheological properties of bituminous binders using the 2S2P1D Model. *Constr. Build. Mater.* **2013**, *38*, 395–406. [CrossRef]
24. Tanakizadeh, A.; Shafabakhsh, G. Viscoelastic characterization of aged asphalt mastics using typical performance grading tests and rheological-micromechanical models. *Constr. Build. Mater.* **2018**, *188*, 88–100. [CrossRef]
25. Rowe, G.; Baumgardner, G.; Sharrock, M. A generalized logistic function to describe the master curve stiffness properties of binder mastics and mixtures. In Proceedings of the 45th Petersen Asphalt Research Conference, Laramie, WY, USA, 14–16 July 2008.

26. Zhang, J.; Pei, J.; Wang, B. Research on time-temperature-stress equivalence principle for asphalt mixture. In Proceedings of the ICCTP 2010: Integrated Transportation Systems: Green, Intelligent, Reliable, Beijing, China, 4–8 August 2010; pp. 3516–3523.
27. Shook, J.; Kallas, B.; McLeod, N.; Finn, F.; Pell, P.; Krchma, L.; Haas, R.; Anderson, K. Factors influencing dynamic modulus of asphalt concrete. In Proceedings of the Association of Asphalt Paving Technologists, Washington, DC, USA, February 1969.
28. Rowe, G.; Baumgardner, G.; Sharrock, M. Functional forms for master curve analysis of bituminous materials. In *Advanced Testing and Characterization of Bituminous Materials, Two Volume set*; CRC Press: Boca Raton, FL, USA, 2009; pp. 97–108.
29. Zhang, F.; Wang, L.; Li, C.; Xing, Y. Predict the Phase Angle Master Curve and Study the Viscoelastic Properties of Warm Mix Crumb Rubber-Modified Asphalt Mixture. *Materials* **2020**, *13*, 5051. [CrossRef] [PubMed]
30. Dickinson, E.J.; Witt, H.P. The Dynamic Shear Modulus of Paving Asphalts as a Function of Frequency. *Trans. Soc. Rheol.* **1974**, *18*, 591–606. [CrossRef]
31. CholewiŃSka, M.; IwaŃSki, M.; Mazurek, G. The Impact of Ageing on the Bitumen Stiffness Modulus Using the Cam Model. *Balt. J. Road Bridge Eng.* **2018**, *13*, 34–39. [CrossRef]
32. Falchetto, A.C.; Moon, K.H.; Wang, D.; Park, H.-W. A modified rheological model for the dynamic modulus of asphalt mixtures. *Can. J. Civ. Eng.* **2021**, *48*, 328–340. [CrossRef]
33. Chen, H.; Barbieri, D.M.; Zhang, X.; Hoff, I. Reliability of Calculation of Dynamic Modulus for Asphalt Mixtures Using Different Master Curve Models and Shift Factor Equations. *Materials* **2022**, *15*, 4325. [CrossRef] [PubMed]
34. Forough, S.A.; Moghadas Nejad, F.; Khodaii, A. An investigation of different fitting functions to accurately model the compressive relaxation modulus master curve of asphalt mixes. *Road Mater. Pavement Des.* **2015**, *16*, 767–783. [CrossRef]
35. Su, N.; Xiao, F.; Wang, J.; Amirkhanian, S. Precision Analysis of Sigmoidal Master Curve Model for Dynamic Modulus of Asphalt Mixtures. *J. Mater. Civ. Eng.* **2018**, *30*, 04018290. [CrossRef]
36. Lachance-Tremblay, É.; Vaillancourt, M.; Perraton, D.; Di Benedetto, H. Linear viscoelastic (LVE) properties of asphalt mixtures with different glass aggregates and hydrated lime content. *Int. J. Pavement Eng.* **2020**, *21*, 1170–1179. [CrossRef]
37. Yusoff, N.I.M.; Airey, G.D.; Hainin, M.R. Predictability of Complex Modulus Using Rheological Models. *Asian J. Sci. Res.* **2009**, *3*, 18–30. [CrossRef]
38. Zbiciak, A.; Michalczyk, R. Characterization of the Complex Moduli for Asphalt-aggregate Mixtures at Various Temperatures. *Procedia Eng.* **2014**, *91*, 118–123. [CrossRef]
39. Yin, Y.; Huang, W.; Lv, J.; Ma, X.; Yan, J. Unified Construction of Dynamic Rheological Master Curve of Asphalts and Asphalt Mixtures. *Int. J. Civ. Eng.* **2017**, *16*, 1057–1067. [CrossRef]
40. Li, Q.; Wang, F.; Forson, K.; Zhang, J.; Zhang, C.; Chen, J.; Xu, N.; Wang, Y. Affecting analysis of the rheological characteristic and reservoir damage of CO2 fracturing fluid in low permeability shale reservoir. *Environ. Sci. Pollut. Res.* **2022**, *29*, 37815–37826. [CrossRef] [PubMed]
41. Li, Q.; Wu, J. Factors affecting the lower limit of the safe mud weight window for drilling operation in hydrate-bearing sediments in the Northern South China Sea. *Geomech. Geophys. Geo Energy Geo Resour.* **2022**, *8*, 82. [CrossRef]
42. Song, X.; Zeng, M.; Fan, L. Relationship among dynamic properties of pavement asphalt materials. *J. Build. Mater* **2018**, *21*, 920–925.
43. Nobakht, M.; Sakhaeifar, M.S. Dynamic modulus and phase angle prediction of laboratory aged asphalt mixtures. *Constr. Build. Mater.* **2018**, *190*, 740–751. [CrossRef]
44. Rahman, A.S.M.A.; Tarefder, R.A. Dynamic modulus and phase angle of warm-mix versus hot-mix asphalt concrete. *Constr. Build. Mater.* **2016**, *126*, 434–441. [CrossRef]
45. Kassem, H.; Chehab, G.; Najjar, S. Effect of Asphalt Mixture Components on the Uncertainty in Dynamic Modulus Mastercurves. *Transp. Res. Rec. J. Transp. Res. Board* **2020**, *2674*, 135–148. [CrossRef]
46. Primusz, P.; Toth, C. Use of the Modified Ramberg-Osgood Material Model to Predict Dynamic Modulus Master Curves of Asphalt Mixtures. *Materials* **2023**, *16*, 531. [CrossRef]
47. You, Z.; Goh, S.W.; Dong, J. Predictive models for dynamic modulus using weighted least square nonlinear multiple regression model. *Can. J. Civ. Eng.* **2012**, *39*, 589–597. [CrossRef]
48. Yang, X.; You, Z. New Predictive Equations for Dynamic Modulus and Phase Angle Using a Nonlinear Least-Squares Regression Model. *J. Mater. Civ. Eng.* **2015**, *27*, 04014131. [CrossRef]
49. Corrales-Azofeifa, J.P.; Archilla, A.R. Dynamic modulus model of hot mix asphalt: Statistical analysis using joint estimation and mixed effects. *J. Infrastruct. Syst.* **2018**, *24*, 04018012. [CrossRef]
50. Hilal, M.M.; Fattah, M.Y. Evaluation of Resilient Modulus and Rutting for Warm Asphalt Mixtures: A Local Study in Iraq. *Appl. Sci.* **2022**, *12*, 12841. [CrossRef]
51. Kadhim, A.J.; Fattah, M.Y.; Asmael, N.M. Evaluation of the moisture damage of warm asphalt mixtures. *Innov. Infrastruct. Solut.* **2020**, *5*, 54. [CrossRef]
52. Chen, Y.; Li, J.; Lu, J.; Ding, M.; Chen, Y. Synthesis and properties of Poly(vinyl alcohol) hydrogels with high strength and toughness. *Polym. Test.* **2022**, *108*, 107516. [CrossRef]
53. Lu, J.; Chen, Y.; Ding, M.; Fan, X.; Hu, J.; Chen, Y.; Li, J.; Li, Z.; Liu, W. A 4arm-PEG macromolecule crosslinked chitosan hydrogels as antibacterial wound dressing. *Carbohydr. Polym.* **2022**, *277*, 118871. [CrossRef]
54. Zhang, Q.; Wang, S.; Lv, R.; Wu, J.; Qi, H. Viscoelastic mechanical performance of dense polyurethane mixtures based on dynamic and static modulus testing and creep testing. *Constr. Build. Mater.* **2022**, *320*, 126207. [CrossRef]

55. Zhao, H.; Zhang, W.; Cui, S.; Ma, S.; Miao, B.; Di, E.; Wang, X.; Su, C.; Wei, J.; Liu, S. Study on the Influence Factors of Dynamic Modulus and Phase Angle of Dense Gradation Polyurethane Mixture. *Coatings* **2023**, *13*, 474. [CrossRef]
56. El-Badawy, S.; Abd El-Hakim, R.; Awed, A. Comparing artificial neural networks with regression models for hot-mix asphalt dynamic modulus prediction. *J. Mater. Civ. Eng.* **2018**, *30*, 04018128. [CrossRef]
57. Yang, R.C.; Kozak, A.; Smith, J.H.G. The potential of Weibull-type functions as flexible growth curves. *Can. J. For. Res.* **1978**, *8*, 424–431. [CrossRef]
58. Richards, F.J. A flexible growth function for empirical use. *J. Exp. Bot.* **1959**, *10*, 290–301. [CrossRef]
59. Marateanu, M.; Anderson, D. Time-temperature dependency of asphalt binders—An improved model (with discussion). *J. Assoc. Asph. Paving Technol.* **1996**, *65*, 408–448.
60. Zeng, M.; Bahia, H.U.; Zhai, H.; Anderson, M.R.; Turner, P. Rheological modeling of modified asphalt binders and mixtures (with discussion). *J. Assoc. Asph. Paving Technol.* **2001**, *70*, 403–441.
61. Fan, B.; Kazmer, D.O. Low-temperature modeling of the time-temperature shift factor for polycarbonate. *Adv. Polym. Technol.* **2005**, *24*, 278–287. [CrossRef]
62. Hutcheson, S.A.; McKenna, G.B. The measurement of mechanical properties of glycerol, m-toluidine, and sucrose benzoate under consideration of corrected rheometer compliance: An in-depth study and review. *J. Chem. Phys.* **2008**, *129*, 074502. [CrossRef] [PubMed]
63. Vestena, P.M.; Schuster, S.L.; Borges de Almeida Jr, P.O.; Faccin, C.; Specht, L.P.; Pereira, D.d.S. Dynamic modulus master curve construction of asphalt mixtures: Error analysis in different models and field scenarios. *Constr. Build. Mater.* **2021**, *301*, 124343. [CrossRef]
64. Oshone, M.; Dave, E.; Daniel, J.S.; Rowe, G.M. Prediction of phase angles from dynamic modulus data and implications for cracking performance evaluation. *Road Mater. Pavement Des.* **2017**, *18*, 491–513. [CrossRef]
65. Rahman, A.S.M.A.; Tarefder, R.A. Viscosity-Based Complex Modulus and Phase-Angle Predictive Models for the Superpave Asphalt Mixtures of New Mexico. *J. Mater. Civ. Eng.* **2018**, *30*, 04018019. [CrossRef]
66. Ceylan, H.; Schwartz, C.W.; Kim, S.; Gopalakrishnan, K. Accuracy of predictive models for dynamic modulus of hot-mix asphalt. *J. Mater. Civ. Eng.* **2009**, *21*, 286–293. [CrossRef]
67. Singh, D.; Zaman, M.; Commuri, S. Evaluation of predictive models for estimating dynamic modulus of hot-mix asphalt in Oklahoma. *Transp. Res. Rec.* **2011**, *2210*, 57–72. [CrossRef]
68. Yusoff, N.I.M.; Jakarni, F.M.; Nguyen, V.H.; Hainin, M.R.; Airey, G.D. Modelling the rheological properties of bituminous binders using mathematical equations. *Constr. Build. Mater.* **2013**, *40*, 174–188. [CrossRef]
69. Booij, H.C.; Thoone, G.P.J.M. Generalization of Kramers-Kronig transforms and some approximations of relations between viscoelastic quantities. *Rheol. Acta* **1982**, *21*, 15–24. [CrossRef]
70. Medani, T.; Huurman, M. *Constructing the Stiffness Master Curves for Asphaltic Mixes*; Delft University of Technology: Delft, The Netherlands, 2003.
71. Nyamuhokya, T.P.; Romanoschi, S.; Hu, X.; Abdullah, A.; Walubita, L.F. Preliminary investigation of the relationship between HMA compressive and tensile dynamic modulus. *Constr. Build. Mater.* **2016**, *128*, 461–470. [CrossRef]
72. Zhang, J.; Bao, L. Determination of asphalt mixture's viscoelastic constitutive parameters for pavement response analysis using dynamic modulus transformation. *Constr. Build. Mater.* **2022**, *315*, 125729. [CrossRef]
73. Xiao, L.; Liang, N.; Chen, L. Dynamic modulus and time-temperature equivalence equation of asphalt concrete. *J. Chang. Univ. (Nat. Sci. Ed.)* **2014**, *34*, 35–40.
74. Guo, L.; Xu, Q.; Zeng, G.; Wu, W.; Zhou, M.; Yan, X.; Zhang, X.; Wei, J. Comparative Study on Complex Modulus and Dynamic Modulus of High-Modulus Asphalt Mixture. *Coatings* **2021**, *11*, 1502. [CrossRef]
75. Shijie, M.; Liang, F.; Tao, M.; Zhao, D.; Yuzhen, Z.; Xiaomeng, Z. Dynamic Characteristic Master Curve and Parameters of Different Asphalt Mixtures. *Appl. Sci.* **2022**, *12*, 3619. [CrossRef]

Disclaimer/Publisher's Note: The statements, opinions and data contained in all publications are solely those of the individual author(s) and contributor(s) and not of MDPI and/or the editor(s). MDPI and/or the editor(s) disclaim responsibility for any injury to people or property resulting from any ideas, methods, instructions or products referred to in the content.